Quasiparticle Dynamics in Disordered Superconductors

Modeling the Single Photon Response

Thomas Rugers

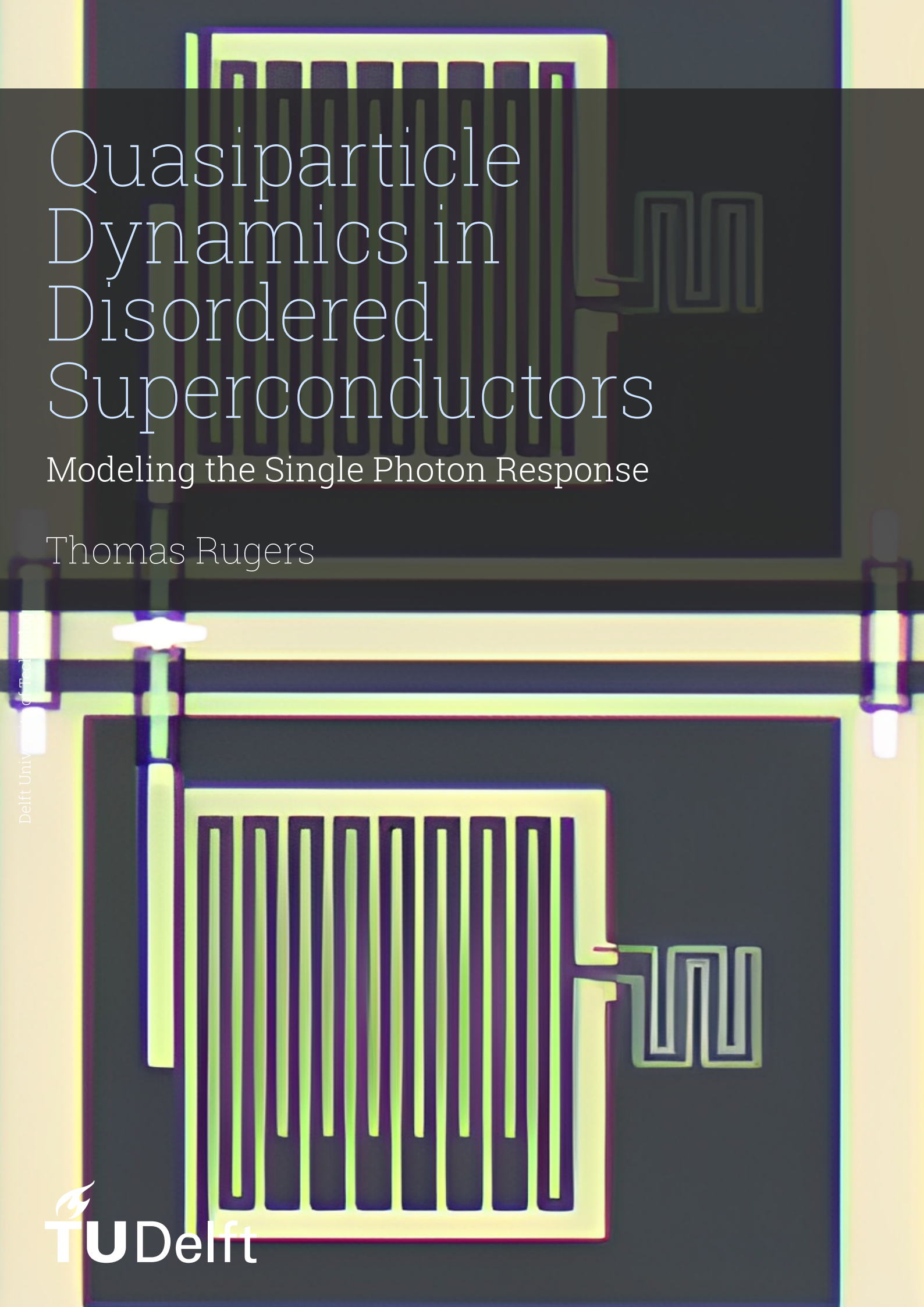

TU Delft

Quasiparticle Dynamics in Disordered Superconductors

Modeling the Single Photon Response

by

Thomas Rugers

Student number:	5167825
Daily supervisor:	Ir. S. A. H. de Rooij
Supervisor:	Prof. dr. ir. J. J. A. Baselmans
Project Duration:	October, 2022 - December, 2022
Faculty:	Faculty of Applied Sciences, TU Delft

Cover: LEKID schematic by [1] (Modified)

TU Delft

Preface

Three years ago I first stepped foot in the TU Delft after freshly coming out of high school. The fact that physics is interesting was clear to me but what it meant to practice physics I had yet to see. Learning all the basic physics in the bachelor courses is important but working on my bachelor's thesis I saw what it means to be a scientist. To do research is a hard task that requires a lot of determination and leaves no room for not being thorough.
I am still standing at the beginning of a whole journey but I want to thank Steven for giving me a first look into the world of research, thank you for always being able to make time and have endless discussions with me. I also want to thank Jochem and Pieter for giving great advice and making sure I wouldn't get ahead of myself. And lastly, I would like to thank my parents for their ever-lasting support throughout my whole bachelor's.

Thomas Rugers
Delft, December 2022

Abstract

Magnetic Kinetic Inductance Detectors (MKIDs) are very good radiation detectors which are even capable of single photon detection in the near-infra red and higher frequency range. MKIDs are currently used to detect exoplanets and the goal is to also retrieve information of the atmosphere of exoplanets. However, MKIDs don't have the photon absorption efficiency and resolving power to do this yet.

In this thesis we look at the single photon pulses of a new superconducting material, beta phased tantalum (β-Ta), since this material shows promising properties for MKIDs. The single photon pulse shapes of this material are not yet fully understood. Therefore we will create models for the quasiparticle dynamics in β-ta to try and further our understanding of the single photon pulses in this material.
From the Rothwarf-Taylor equations we derive multiple models. These are then tested on the data. We first try the double exponential model which does not work. Then we look at the $1/t$ model and this model does seem to work better. We propose a different response time of the system. Fitting a new response time we get a very good fit to the single photon pulses. The main hypothesis is that there is an extra relaxation time for the quasiparticles as they need to distribute themselves throughout the superconductor. We see that the fitted response time is wavelength dependent which would support the hypothesis.
We conclude that the $1/t$ model with an adjusted response time explains the single photon pule shapes the best.

Contents

1 Introduction

Since the beginning of time humanity has been curious about the world around us. This is why Christopher Columbus and Marco Polo were exploring the globe and Isaac Newton was figuring out the mathematical rules of nature. But maybe the most interesting question of all was about that starry night sky that riddled humanity every time they looked at it.
First people started making observations with their bare eyes. However, the eyes don't make for very precise measuring instruments. When Galileo Galilei made the first telescope in 1610 he made a big contribution to observing space but he was still dependent on his eyes. But a really big change came in 1905 when Einstein proposed that light consisted of quantized energy bundles that this changed. An electrical device could now detect light with the photoelectric effect. From here detectors could be made, where firstly single photon detection became possible with photomultiplier tubes.
For astronomy before the 80s mostly photographic plates were used. After that, because of their very high quantum efficiencies, the charged coupled devices (CCD) and the complementary metal–oxide–semiconductor (CMOS) became the standard [2]. Most notably the Hubble telescope uses these detectors.

Next, the discovery of superconductors created the gateway to a new type of detector. These detectors are called Microwave Kinetic Inductance Detectors (MKIDs) and they can measure very small energy disturbances. Small enough so that the measurement of a single photon in the range of visible light is possible. An image of an MKID array can be found in figure 1.1. The MKID can also then determine the wavelength of the photon that it measures. MKIDs are already being used to observe distant galaxies in the Deep Spectroscopic High-redshift Mapper (DESHIMA) project. Here the MKIDs are used as a power integrating detector in the Atacama Submillimeter Telescope Experiment (ASTE) in Chile so we can find out more about the history of the universe [3].
The next step will be to get an MKID-based sensor into space with a satellite to remove atmospheric distortion. This would make it among other things possible for MKIDs to measure the atmosphere of exoplanets enabling it to research their habitability.

However, there are still some hurdles with the usage of MKIDs that need to be overcome. The most common superconducting material that is used in MKIDs is Aluminium. This is a well-understood superconductor but some of its properties make it hard to use as a sensor.
Firstly its photon absorption efficiency is low. This is the percentage of photons that get absorbed into the superconductor as some of the photons will get reflected off or pass right through the material.
Secondly, the energy-resolving power for photons is not sufficient yet for exoplanet atmosphere spectroscopy. These two reasons make it a problem to use the MKID effectively.

This is the reason that we are looking into new superconducting materials. One of these is β-phased Tantalum (β-Ta), a disordered superconductor. The behavior of this superconductor however is very different from Aluminium. We are looking at the behavior of a single photon pulse. Some examples of these can be found in the right picture of figure 1.1. These single photon pulse shapes are different from Aluminium and inconsistent with the old theory. Understanding these shapes would mean that

the material can be used effectively in the MKIDs.
That's why in this thesis the single photon pulse shape of β-Tantalum will be researched. The goal is to understand the quasiparticle dynamics in the superconductor by making a model that will fit the single photon pulses.
In chapter two first the theory behind superconductivity will be explained and then quasiparticle dynamics and the working of MKIDs. In the third chapter different models to explain the single photon pulse of an MKID will be presented and looked at. Then in the fourth chapter, these models will be tested with the single photon pulses that were measured from the β-Ta MKIDs. Finally in chapter five conclusions will be made together with recommendations for future work.

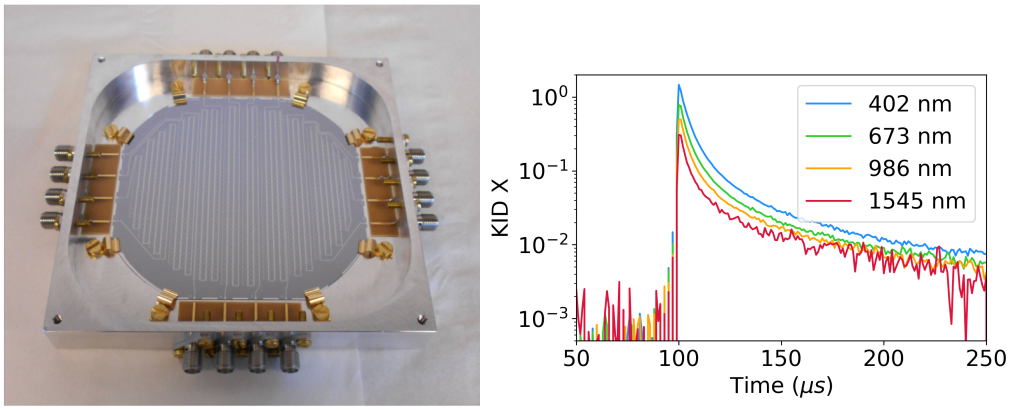

Figure 1.1: On the left is an image of the NIKA-2 MKID array. And in the right graph are examples of averaged single photon pulses measured on Chip 2, KID 2 at different wavelength photon pulses at a temperature of 18 mK and with a read-out power of -105 dBm.

2

Theory

2.1. Superconductivity

In 1911 Dutch physicist Heike Kamerlingh Onnes cooled mercury down to 4.2 Kelvin using liquid Helium, where he researched the properties of metals at low temperatures. He observed a complete vanishing of electrical resistance [4]. It was not until 1957 that a complete theory was made for superconductivity, the Bardeen–Cooper–Schrieffer (BCS) theory. This theory will be discussed on a surface level here with the necessary knowledge for this thesis.

In BCS theory Leon Cooper showed that free electrons in metals at low temperatures are unstable and can form pairs if there is an attractive potential. As long as there is an attractive potential, even if it is very weak the electrons will pair up into so-called Cooper pairs. The binding energy of a Cooper pair is given by $2\Delta = 3.52 k_B T_c$. Where k_B is the Boltzmann constant and T_c is the critical temperature.
In metals, the attractive potential is generally explained by the deformation of the lattice due to the electron as shown in figure 2.1. As one electron deforms the lattice by attracting the positively charged atoms it creates a small more positively charged region. This then creates an attractive potential for another electron making the electrons pair up. All the electrons which are fermions pair up with each other becoming bosons. this enables them to all be in the same state. So the electrons form a condensate basically becoming an electron superfluid.[5], [6]

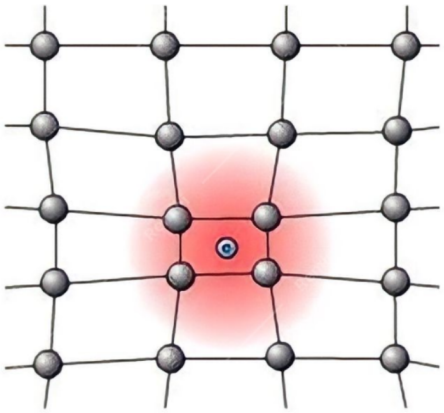

Figure 2.1: The deformation of the lattice in a metal because of an electron creating a positive charge density in the vicinity. Figure from [7]

These Cooper pairs induce all of the superconductor properties. The most important one is the vanishing of the electrical resistance. As all the electrons have become a condensate they move through the lattice without any dissipation. Accelerating the electrons is then only limited by their inertia giving rise to kinetic inductance.

At non-zero temperatures, there will still be phonons with an energy equal to or greater than 2Δ in the material which can break the Cooper pairs. When a Cooper pair breaks it splits up into two quasiparticles. These are a superposition of an electron and a hole (a positively charged region that indicates the lack of an electron at a certain position) which can be viewed as a single fermion. While phonons are breaking the quasiparticles, recombination of quasiparticles into Cooper pairs is also possible. Depending on the temperature there will be a certain density of quasiparticles in the material at equilibrium. This is given by,

$$n_{qp} = 4N_0 \int_0^\infty f\left(E; k_B T\right) N_s(E) dE = 4N_0 \int_\Delta^\infty \frac{f\left(E; k_B T\right) E}{\sqrt{E^2 - \Delta^2}} dE, \tag{2.1}$$

where N_0 is the electron density of states at the Fermi level, $f\left(E; k_B T\right)$ is the quasiparticle distribution, and $N_s(E) = \Re\left(\frac{E}{\sqrt{E^2-\Delta^2}}\right)$ is the normalized BCS quasiparticle density of states. By multiplying this density with the volume of the superconductor you will obtain the total amount of thermal quasiparticles: $N_{qp}^0 = n_{qp}^0 V$
In this equation, as the temperature goes up the number of quasiparticles goes up too.
Then if the Fermi-Dirac distribution is used and low temperatures are considered ($k_b T \ll \Delta$), n_{qp} can be approximated by [8],

$$n_{qp} \approx 2N_0 \sqrt{2\pi k_b T \Delta} e^{-\Delta / k_b T}, \tag{2.2}$$

Up until now, only the thermal equilibrium has been looked at but for MKIDs it is necessary to look at the case where the amount of quasiparticles is disturbed out of thermal equilibrium. This is the case when a photon hits the superconductor and breaks the Cooper pairs up into quasiparticles. In the next section, these quasiparticle dynamics will be looked at.

2.2. Quasiparticle dynamics

As quasiparticles recombine into a Cooper pair they release a phonon, and the other way around a phonon can be absorbed by a Cooper pair to break it which in turn generates quasiparticles. So one can write master equations considering the phonons of the system and quasiparticles.
The equations that describe this are called the Rothwarf-Taylor equations [9] which are coupled non-linear differential equations given by,

$$\begin{aligned} \frac{dN_{qp}}{dt} &= -\frac{RN_{qp}^2}{V} + 2\Gamma_B N_\omega, \\ \frac{dN_\omega}{dt} &= \frac{1}{2}\frac{RN_{qp}^2}{V} - \Gamma_B N_\omega - \Gamma_{es} N_\omega + \Gamma_K N_{\omega,B}, \\ \frac{dN_{\omega,B}}{dt} &= \Gamma_{es} N_\omega - \Gamma_K N_{\omega,B}. \end{aligned} \tag{2.3}$$

Here the system is made up of three levels. Firstly there is the number of quasiparticles N_{qp} which interacts with the phonons in the superconductor N_ω which is the second level. The phonons considered are only the ones with energy $\Omega \geq 2\Delta$ which can break the Cooper pairs. The last level is made up of the phonons in the cooling bath to which the superconductor is connected.
The first line of the equations looks at the change in the number of quasiparticles. First, there is a recombination term which is quadratic since they combine as a pair into a Cooper pair. Here R is the recombination constant. Then for the second creation term phonons can break the Cooper pairs and create quasiparticles, this is dependent on the pair breaking rate $\Gamma_B = 1/\tau_{pb}$ and the number of phonons.
The second line of the equation gives the change in pair-breaking phonons and the first term is the same quadratic term that appears in the quasiparticle equation since at the same time a phonon is created. However, for two quasiparticles, one phonon is created which explains the factor $1/2$. The same goes for the second term. The last two terms are about the phonons escaping into the bath and coming from the bath back into the superconductor. Here $\Gamma_{es} = 1/\tau_{es}$ and Γ_K are the phonon escape rate into the bath and the rate at which the bath phonons enter the superconductor from the phonon bath respectively.
The last equation looks at the phonons in the bath which go up if a phonon escapes into it and go down

when one goes back into the superconductor.

Since the bath is so much bigger than the superconductor the photons from the bath are basically always in equilibrium. Setting the bath phonons constant we find that $\Gamma_{es}N_\omega^0 = \Gamma_K N_{\omega,B}^0$. From this, we end up with two equations, one for the quasiparticles and one for the pair-breaking phonons. In this thesis, zero as a superscript means that it is a steady state value or thermal equilibrium value.

$$\begin{aligned}\frac{dN_{qp}}{dt} &= -\frac{RN_{qp}^2}{V} + 2\Gamma_B N_\omega \\ \frac{dN_\omega}{dt} &= \frac{RN_{qp}^2}{2V} - \Gamma_B N_\omega - \Gamma_{es}\left(N_\omega - N_\omega^0\right).\end{aligned} \tag{2.4}$$

The first term in both of the equations in 2.4 is still the recombination of quasiparticles. Then the second term is the pair breaking by the phonons and the last term in the phonon equation is the escaping of phonons into the phonon bath. These equations do not have an analytical solution (yet) so to solve them certain assumptions have to be made. There are two limits in which these equations can be solved. The first is when there is a large number of excess quasiparticles ($\delta N_{qp} \gg N_{qp}^0$), this means that recombination will be dominant so we can ignore the pair-breaking term and solve the quasiparticle equation,

$$\frac{dN_{qp}}{dt} = -\frac{RN_{qp}^2}{V} \qquad \Rightarrow \qquad \int \frac{1}{N_{qp}^2} dN_{qp} = -\int \frac{R}{V} dt \qquad \Rightarrow \qquad N_{qp}(t) = N_{qp}(0)\frac{\frac{R}{V}}{N_{qp}(0)t + \frac{R}{V}}.$$

Where first the terms are moved around to separate the variables and then it is integrated on both sides. From the result, it can be seen that in the regime where there is a high amount of excess quasiparticles the recombination of quasiparticles has a dependence of $\propto 1/t$. This regime is when $T << T_c$ and thus the amount of thermal quasiparticles is very low. If a photon hits the superconductor in this regime the number of excess quasiparticles will be very big compared to the thermal quasiparticles. We will call this the low-temperature regime.
The other regime is when the amount of excess quasiparticles is very small. Then a linearization can be made to find that the amount of excess quasiparticles is a single exponential, $\delta N_{qp} \propto e^{-2t/\tau_{qp}}$, where $\tau_{qp} = 1/\Gamma_R = V/RN_{qp}^0$ is the single quasiparticle lifetime. An in-depth derivation of this will be done in the next chapter.

There has been a calculation of the single quasiparticle lifetime done by Kaplan [10]. He showed that when using the Fermi-Dirac distribution for low temperature and quasiparticles of energy Δ is,

$$\tau_{qp} = \frac{\tau_0}{\sqrt{\pi}}\left(\frac{k_B T_c}{2\Delta}\right)^{5/2}\sqrt{\frac{T_c}{T}}e^{\Delta/k_B T} = \frac{V\tau_0}{N_{qp}^0}\frac{N_0\left(k_B T_c\right)^3}{2\Delta^2}, \tag{2.5}$$

where τ_0 is an electron-phonon interaction time, which is a material parameter. Its shows that the lifetime of the quasiparticles is inversely proportional to the quasiparticle number itself. For low temperatures we expect the quasiparticle lifetime to be very high. Equation 2.5 gives us the means to calculate the quasiparticle lifetime by theory and also the recombination constant as they are connected by $R = V/\tau_{qp}N_{qp}^0$.

2.3. Kinetic Inductance Detectors

Now that we know the basics of superconductivity and quasiparticle dynamics we can take a look at how the MKIDs are used as a light detectors. In an MKID the superconductor is placed into a microwave resonator. The superconductor is capacitively coupled to a read-out line with which the signal is read out at Gigahertz frequencies.
So the question is how the superconductor reacts to an external alternating electrical field. For this we can use Ohm's law, $\boldsymbol{j} = \sigma \boldsymbol{E}$. Here we define two parts of the conductivity, $\sigma = \sigma_1 - j\sigma_2$, where the first real part σ_1 is the dissipative part and the second imaginary part σ_2 is the inductance part. The dissipative part is coupled to the quasiparticles which still have electrical resistance and the inductance part is coupled to the inertia of the Cooper pairs and is thus called kinetic inductance. As a photon hits

the superconductor the number of quasiparticles and Cooper pairs change which induces a change in σ_1 and σ_2.

Through the read-out line runs a certain power also called the read-out power. Since this line is coupled to the superconductor part of its power is transferred to the superconductor by accelerating the quasiparticles and Cooper pairs. As the inductive, resistive, and capacitive parts make up an RLC circuit it has a certain resonance frequency at which maximum power is transferred to the superconductor. We will sweep the frequency to find the resonance frequency of the resonator. The resonator will then be driven at its resonance frequency.

An overview of the MKID working principle is given in figure 2.2. Figure 2.2(a) first shows a Cooper pair breaking into quasiparticles and figure 2.2(b) gives a schematic of the circuit made by the resonator. It can be seen how the read-out line is capacitively coupled to the resonator which has a capacitance, changing induction, and changing resistance with the changing amounts of quasiparticles. Lastly in figure 2.2(c) we can see the change of resonance frequency due to a photon stream hitting the superconductor. The photons break the Cooper pairs into quasiparticles in the superconductor inducing a change in kinetic inductance. With this change, the resonance frequency lowers and the resonance dip decreases. The width of the peak widens because the quality factor decreases. This happens because there are more quasiparticles so the dissipation increases. This change in kinetic inductance and power dissipation is what we measure.

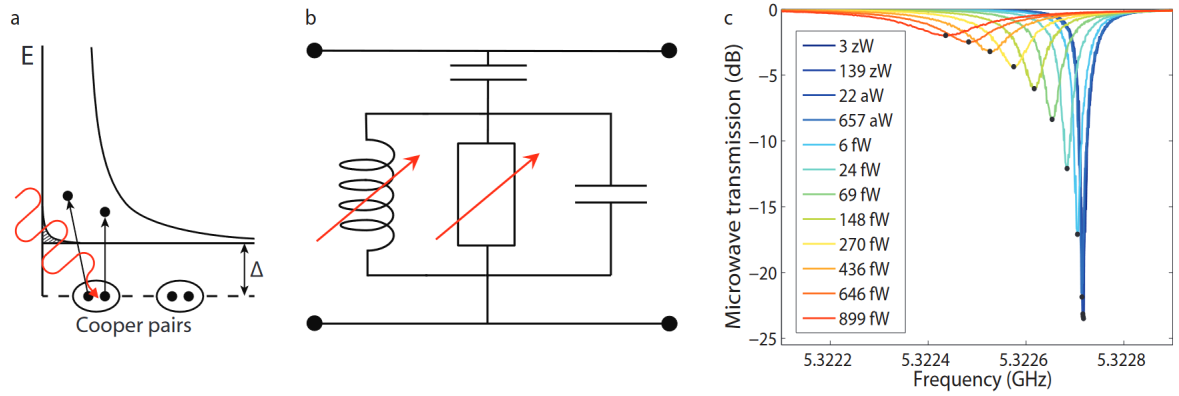

Figure 2.2: An overview of the working principle of MKIDs. In (a) Cooper pairs are broken by an incoming photon of energy $E > 2\Delta$. (b) A simplified circuit of an MKID that shows the read-out line (upper line) being capacitively coupled to the microwave resonator. As the amount of Cooper pairs and quasiparticles change the kinetic inductance and resistance of the resonator also change. (c), The microwave transmission in the read-out line is shown as a function of frequency in the resonator. When a photon is absorbed the resonance frequency shifts because of the change in inductance and the dip decreases as the resistance goes up. The legend shows the applied power on the superconductor at 1.54 THz. figure from [11]

2.3.1. KID Setup

The KIDs looked at for this thesis are Lumped Element KIDs (LEKIDs) that use a high resistivity β-Ta inductor and a NbTiN interdigitated capacitor. A schematic is shown in figure 2.3. The read-out line is the central line in the figure which is a coplanar waveguide (CPW) made of NbTiN. This means that on both sides there is a grounded part running parallel with the supply line. The CPW is then capacitively coupled to the resonator using a coupling bridge. This connects to an interdigitated capacitor made of NbTiN where the length of the fingers in the capacitor changes the resonance frequency for each KID. Finally, the capacitor connects to the inductor made of β-Ta on which the photons will fall changing the resistance and inductance.

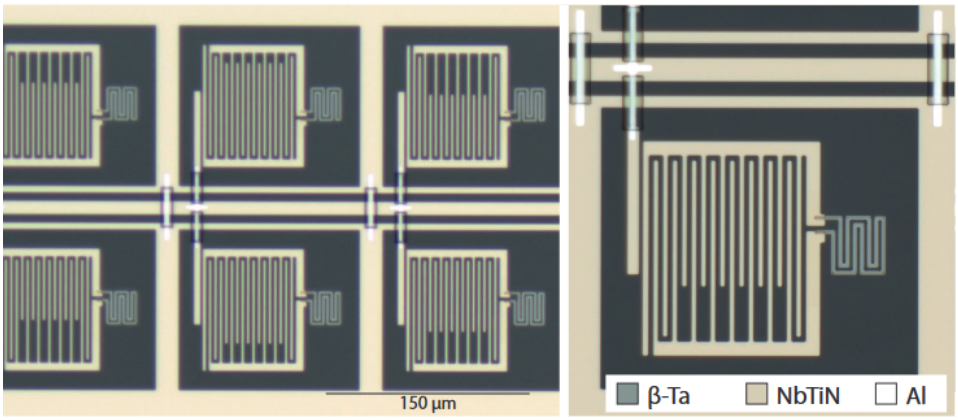

Figure 2.3: A schematic overview of an array of LEKIDs. On the left, we can see six different KIDs coupled to the read-out line on both sides. The ground plane is also connected at regular intervals. On the right, a closer look at one KID can be seen with the NbTiN IDC and the β-Ta inductor. [1]

The chip is cooled down to temperatures below the critical temperature inside a pulse-tubed dilution refrigerator. The setup in this cryostat can be seen in figure 2.4. It consists of multiple temperature stages where the lowest stage is called the 100-mK stage. This stage is shielded from stray light emitted by the 3-K stage. An optical fiber couples laser light into the cryostat which is first thermalized to 3 K. This optical fiber then goes through the shield into a 100-mK box where it first has to go through a diffuser before it enters the 100-mK stage. The diffuser spreads out the light which then hits a BK7 window to only let in light in the visible spectrum to the submillimeter region. After the window, the light will fall onto the detector from where the microwave measurements are made.

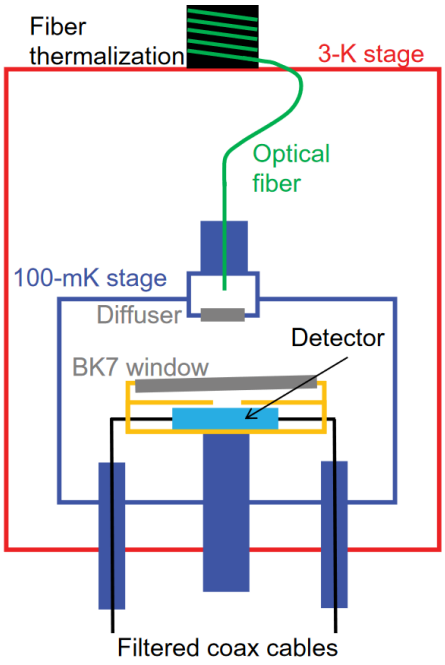

Figure 2.4: A schematic overview of the inner parts of the cryostat, where the different temperature stages can be seen together with the optical setup. Figure from [12]

2.3.2. KID Measurement Coordinates

We now know how the MKID measures the change in resonance frequency and Q-factor by the change in power from the read-out line. But how does one translate this to the change in the number of quasiparticles? Equation 2.2 enables us to calculate an effective quasiparticle temperature from the number of quasiparticles. Mattis and Bardeen [13] showed that from there it is possible to calculate σ_1 and σ_2. So the first step is the connection from the number of quasiparticles to the complex conductivity.

The next question is how the complex conductivity influences the circuit from which we are measuring. This information is captured within the surface impedance, $Z_s = R_s + j\omega L_s$, which is a material property that characterizes its response to an external field at a certain frequency. Here R_s is the surface resistance, L_s is the surface inductance, and ω is the angular frequency of the signal. How these are calculated is explained very well in [11] and are given by,

$$\begin{aligned} R_s &= \mu_0 \omega \frac{\sigma_1}{2\sigma_2} \beta \lambda \coth\left(\frac{d}{\lambda}\right) \\ L_s &= \mu_0 \lambda \coth\left(\frac{d}{\lambda}\right), \end{aligned} \tag{2.6}$$

where λ is the penetration depth, μ_0 the magnetic permeability of vacuum and $\beta = 1 + \frac{2d/\lambda}{\sinh 2d/\lambda}$.
Since the superconductor is part of a resonating circuit the changes in the surface impedance will change the resonance frequency and Q-factor. We can define the internal quality factor as [14],

$$Q_i = \frac{\omega L}{R} = \frac{1}{\alpha_k} \frac{\omega L_s}{R_s} = \frac{2}{\alpha_k \beta} \frac{\sigma_2}{\sigma_1}, \tag{2.7}$$

where $\alpha_k = L_s/L$ is the kinetic induction fraction, where L is the total inductance in the circuit and L_s is the sheet inductance. A higher internal quality factor means that there is less energy lost to accelerating the particles or in other words, there are fewer quasiparticles.
With these equations, we can find how changes in the complex conductivity induce changes in the Q-factor and resonance frequency. For a change in σ it has been shown that [15],

$$\delta\left(\frac{1}{Q_i}\right) \approx \frac{\alpha_k \beta}{2} \frac{\delta\sigma_1}{\sigma_2}, \tag{2.8}$$

where once again the low temperature limit was used, $\sigma_2 \gg \sigma_1$ and $\delta\sigma_1 \gg \delta\sigma_2$. And for the resonance frequency it gives [15]:

$$\frac{\delta\omega_0}{\omega_0} = \frac{\alpha_k \beta}{4} \frac{\delta\sigma_2}{\sigma_2}. \tag{2.9}$$

The last step is how the measured complex transmission is connected to the resonator properties. In figure 2.2(b) we saw a schematic overview of the MKID and from this, the forward transmission can be calculated [16]:

$$S_{21} = \frac{Q/Q_i + 2jQ\frac{\delta\omega}{\omega_0}}{1 + 2jQ\frac{\delta\omega}{\omega_0}}, \tag{2.10}$$

where Q is the loaded quality factor $1/Q = 1/Q_i + 1/Q_c$, with Q_c the coupling quality factor and $\delta\omega = \omega_{read} - \omega_0$. ω_{read} is the driving frequency of the read-out line which is set to the resonance frequency of the resonator.
When the read-out frequency is swept while the KID is kept in equilibrium S_{21} traces out a circle in the complex plane (red circle in figure 2.5). In the limit where $|\delta\omega| \to \infty$ we can see from equation 2.10 that $S_{21} \to 1$ which can also be seen in figure 2.5 which is the most right point of the red circle. The most left point is when $\delta\omega = 0$ which gives $S_{21}^{min} = Q/Q_i$. With this information, we can deduce that the center point of the circle is $x_c = (S_{21}^{min} + 1)/2$.
When making a measurement ω_{read} will be equal to the resonance frequency making $\delta\omega$ equal to zero. So S_{21} will be at its minimum or the most left point in the circle. However when a photon hits the superconductor the resonance frequency and quality factor change. With this S_{21} will change. This is shown with the blue dots in figure 2.5 where we can see that the radius of the circle changes and S_{21} moves on the circle with a certain phase.

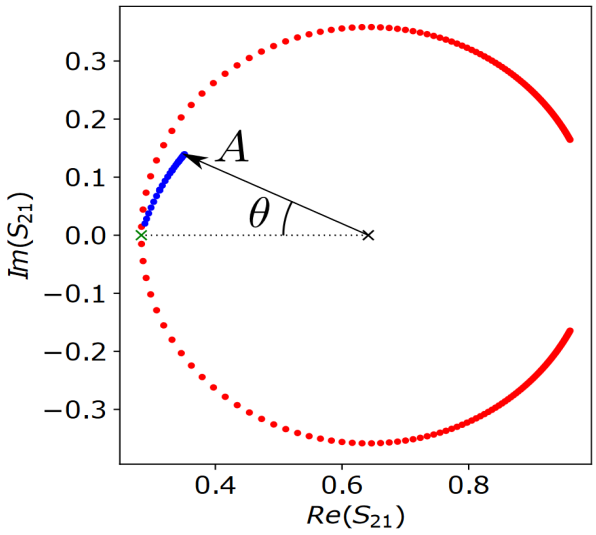

Figure 2.5: [15]

In general, these changes are described by the coordinates amplitude (A) and phase (θ) with respect to the center point of the circle. These are given by,

$$\begin{aligned} A &= \frac{\sqrt{\left(\Re\left(S_{21}\right)-x_c\right)^2+\Im\left(S_{21}\right)^2}}{1-x_c}, \\ \theta &= \arctan\left(\frac{\Im\left(S_{21}\right)}{x_c-\Re\left(S_{21}\right)}\right). \end{aligned} \tag{2.11}$$

For these coordinates, S. de Rooij [15] calculated the relationship between the changes in the quality factor and resonance frequency and amplitude and phase which are given by,

$$\begin{aligned} \delta A &\approx -2Q\delta\left(\frac{1}{Q_i}\right), \\ \theta &\approx 4Q\frac{\delta\omega}{\omega_0}. \end{aligned} \tag{2.12}$$

Here it was used that $\delta A = 1-A$ and $\tan\theta \approx \theta$. Combining equations 2.12, 2.8, and 2.9 we have finally come full circle and are able to derive the changes from the coordinates with respect to the changes in quasiparticles [11], [14]:

$$\begin{aligned} \frac{dA}{dN_{qp}} &= -\frac{\alpha_k\beta Q}{|\sigma|V}\frac{d\sigma_1}{dn_{qp}}, \\ \frac{d\theta}{dN_{qp}} &= -\frac{\alpha_k\beta Q}{|\sigma|V}\frac{d\sigma_2}{dn_{qp}}. \end{aligned} \tag{2.13}$$

The equations show that the responsivity of the KID is dependent on the factor $\alpha_k\beta Q/|\sigma|V$ for both coordinates. These coordinates, however, are only linear in the small signal limit.

Since these coordinates are only linear for small signals we will use different coordinates for the pulse analysis in this thesis. In the paper of N. Zobrist [17] the authors propose a Smith Chart-like coordinate system which we will call (R,X). The details of this coordinate system can be found in the paper as it surpasses the depth of this thesis but the most important fact is that this coordinate system has a linear response to the photon energy.

In figure 2.6 some data is shown to compare the amplitude and phase coordinates to the R and X coordinates. We are looking at averaged single photon pulses at two different wavelengths on the same chip and KID. The pulse heights have been normalized to their maximum to enable us to compare the

differences in shape. The original pulse heights were around 10^{-1} for the 1545 nm pulse and around 1 for the 402 nm pulse.

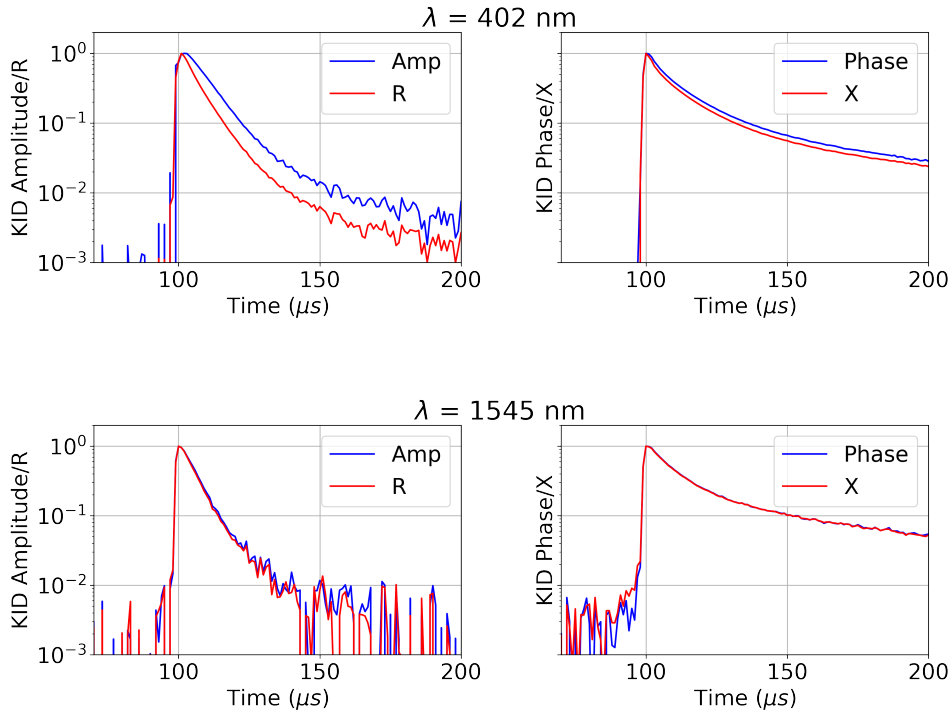

Figure 2.6: Normalised single photon pulses in both the amplitude/phase and the R/X coordinates at two different photon wavelengths. The data is taken from Chip A, KID 2 at a read-out power of -101 dBm and a temperature of 18 mK.

From this figure, we conclude that the difference between amplitude/phase coordinates or R, X coordinates is negligible for low pulses and very small for high pulses. This is why it is chosen to work with only (R,X)-coordinates for the data analysis. To be consistent with the coordinates and to make sure the nonlinearities with respect to the quasiparticle number of amplitude and phase in the high pulse domain don't influence the analysis.

3

Methods and Models

Predicting the behavior of the quasiparticles in the superconductor starts with analyzing the Rothwarf-Taylor equations (equation 2.4. In this chapter, we will look at the different limits of the quasiparticle behavior enabling us to solve the Rothwarf-Taylor equations in these limits. This will give us analytical solutions that can be tested. These will then be compared to the numerical solution of the Rothwarf-Taylor equations

3.1. The Exponential Model

3.1.1. Double Exponential Model

The first model has at its core the limit that the excess amount of quasiparticles created by the photon pulse is a lot smaller than the thermal quasiparticle amount ($\delta N_{qp} \ll N_{qp}^0$). Let us start with the Rothwarf-Taylor equations as in equation 2.4. We can then split the quasiparticle and phonon terms into an equilibrium part and excess part by writing $N_{qp} = N_{qp}^0 + \delta N_{qp}$ and $N_\omega = N_\omega^0 + \delta N_\omega$. If we insert this into equation 2.4 we can then linearize this by discarding the nonlinear terms in δN_{qp} and δN_ω. This results in,

$$\begin{aligned} \frac{d\delta N_{qp}}{dt} &= -\frac{2RN_{qp}^0\delta N_{qp}}{V} + 2\Gamma_B\delta N_\omega, \\ \frac{d\delta N_\omega}{dt} &= \frac{RN_{qp}^0\delta N_{qp}}{V} - (\Gamma_B + \Gamma_{es})\delta N_\omega, \end{aligned} \tag{3.1}$$

where we used that the equilibrium amount of quasiparticles and phonons are the thermal amount ($N_\omega^0 = N_\omega^T$). This can be written down into the following vector equation:

$$\frac{d\mathbf{a}}{dt} = -\Gamma \cdot \mathbf{a} + \mathbf{u}, \quad \Gamma = \begin{pmatrix} 2\Gamma_R & -2\Gamma_B \\ -\Gamma_R & \Gamma_\omega \end{pmatrix}, \tag{3.2}$$

with $\mathbf{a} = (\delta N_{qp}, \delta N_w)$, $\Gamma_R = RN_{qp}^0/V$ and $\Gamma_\omega = \Gamma_B + \Gamma_{es}$. This is a first-order coupled linear differential equation so we assume the solution to be along the line of an exponential or superposition of exponentials: $e^{\lambda t}$. Trying this solution on equation 3.2 we find an eigenvalue problem for the Γ matrix. Solving for the eigenvalues of this matrix we find:

$$\lambda = \frac{2\Gamma_R + \Gamma_\omega \pm \sqrt{(2\Gamma_R + \Gamma_\omega)^2 + 8\Gamma_R(\Gamma_B - \Gamma_\omega)}}{2}. \tag{3.3}$$

This gives us a general solution expression for, for example, the quasiparticles in the system:

$$\delta N_{qp} = Ae^{\lambda_- t} + Be^{\lambda_+ t}, \tag{3.4}$$

where A and B are general constants. We call this the double exponential model.

3.1.2. Single Exponential Model

From here we can make one more assumption to simplify the expression for the eigenvalues. From theory [10] we know that $\Gamma_R \ll \Gamma_B + \Gamma_{es} = \Gamma_\omega$. We will take the slow time λ_- which will be the quasiparticle lifetime. We Taylor expand λ_- in Γ_R around zero to the first-order since it is very small compared to the other terms. First the partial derivative in Γ_R is calculated:

$$\frac{d\lambda_-}{d\Gamma_R} = 1 - \frac{2\Gamma_R + \Gamma_\omega + 2\left(\Gamma_B - \Gamma_\omega\right)}{\sqrt{\left(2\Gamma_R + \Gamma_\omega\right)^2 + 8\Gamma_R\left(\Gamma_B - \Gamma_\omega\right)}}, \tag{3.5}$$

and then using $\lambda_-(\Gamma_R) \approx \lambda_-(0) + \frac{d\lambda_-}{d\Gamma_R}(0)\Gamma_R$ we get:

$$\lambda_-(\Gamma_R) \approx \frac{\Gamma_\omega - \sqrt{\Gamma_\omega^2}}{2} + (1 - \frac{\Gamma_\omega + 2(\Gamma_B - \Gamma_\omega)}{\sqrt{\Gamma_\omega^2}})\Gamma_R. \tag{3.6}$$

Working this out further gives:

$$\Gamma_R^* \approx (1 - \frac{\Gamma_\omega + 2(\Gamma_B - \Gamma_\omega)}{\Gamma_\omega})\Gamma_R = (\frac{2\Gamma_{es}}{\Gamma_\omega})\Gamma_R = 2\Gamma_R(\frac{\Gamma_{es} + \Gamma_B}{\Gamma_{es}})^{-1} = 2\Gamma_R(1 + \frac{\Gamma_B}{\Gamma_{es}})^{-1}. \tag{3.7}$$

Here we called the apparent recombination rate constant of the quasiparticles $\Gamma_R^* = 1/\tau_{qp}^*$. Writing the expression like this gives us some insight into the behavior of the bulk when the phonon system is a lot faster than the quasiparticle system. Firstly the apparent bulk quasiparticle rate is twice as fast since it accounts for both the quasiparticles recombining into a Cooper pair. And secondly, there is the phonon trapping factor which slows down the system. This is because phonons that are emitted by a Cooper pair break another Cooper pair before escaping into the phonon bath.
Thus knowing R and V together with the number of thermal quasiparticles one can use equation 2.5 to calculate Γ_R and from there also calculate Γ_R^*. For these approximations we are left with only one exponential decay thus we call it the single exponential model.

To test these models graphs are made of the analytical exponential model versus a numerical solution of the Rothwarf-Taylor equations. This is done to test the limits of the model. The two limits are the low-temperature limit and the phonon times versus the quasiparticle times. In figure 3.1 we first take a look at the temperature limit. The variables taken for the model are given in the appendix. At 200 mK the single exponential model is very close to the numerical solution. However, at 100 mK the numerical solution has a completely different shape compared to the single exponential model. It is clear that at the beginning of the pulse shape the $1/t$ behavior is dominating.

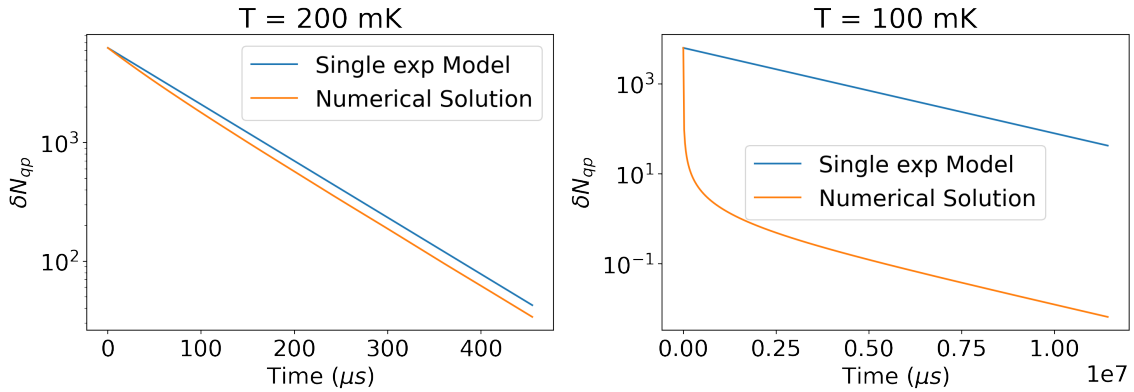

Figure 3.1: A comparison of the Single exponential model with a numerical solution of the Rothwarf-Taylor equations for different temperatures.

Secondly, we assumed the phonon lifetimes the be a lot slower than the quasiparticle lifetimes. If this is not true then the single exponential model should turn into the double exponential model. This is exactly what we see in figure 3.2. In the left graph, it is first looked at the case if only one of the lifetimes

is a lot slower. But we can see, here the model still works. Then on the right, it shows the case where both the phonon lifetimes are not a lot faster than the quasiparticle lifetime. This confirms that for the model to work just one of the phonon lifetimes has to be a lot faster than the quasiparticle lifetime. So if just the pair breaking time or the escape time is a lot slower than the quasiparticle lifetime then that doesn't break the limit as $\Gamma_B + \Gamma_{es}$ is still bigger than Γ_R. They both have to be slow to break the limit.

One thing that has to be noted is the fact that for the double exponential model the two lifetimes are not the quasiparticle and phonon lifetimes. We don't decouple the systems by stating that one of the two is a lot faster. This means that there is no single lifetime for either of the systems as they are coupled.

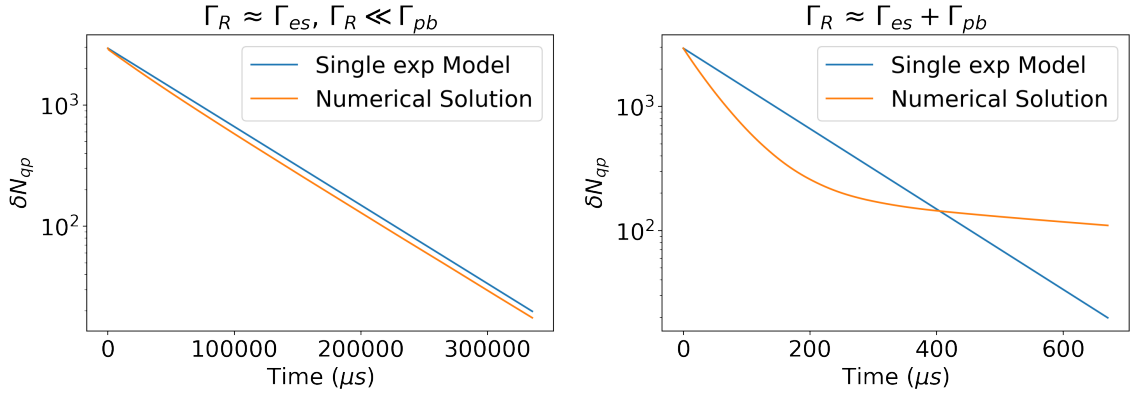

Figure 3.2: A comparison of the Single exponential model with a numerical solution of the Rothwarf-Taylor equations for different escape and pair breaking times.

3.2. The $1/t$ model

The next model will attempt to capture both the exponential and the $1/t$ behavior of the quasiparticle decay, as explained in the previous chapter. This means this model has to work in both the high and low-temperature limits. We start with the same strategy as was used in the exponential model where we split the number of quasiparticles and phonons into an equilibrium (steady state) value plus an excess amount of particles. However here a linearization can't be made since the approximation that $\delta N_{qp} \ll N_{qp}^0$ is not true. Substituting this into the Rothwarf-Taylor equations and rewriting we get the following coupled nonlinear differential equations.

$$\begin{aligned} \frac{d\delta N_{qp}}{dt} &= -\frac{R}{V}\delta N_{qp}^2 - 2\Gamma_R \delta N_{qp} + 2\Gamma_B \delta N_\omega, \\ \frac{d\delta N_\omega}{dt} &= \frac{R}{2V}\delta N_{qp}^2 + \Gamma_R \delta N_{qp} - (\Gamma_B + \Gamma_{es})\delta N_\omega, \end{aligned} \tag{3.8}$$

where Γ_R is the same as before. We notice that the equations are almost symmetrical so we sum the first line with twice the second line and we get,

$$\frac{d\delta N_{qp}}{dt} + 2\frac{d\delta N_\omega}{dt} = -2\Gamma_{es}\delta N_\omega \tag{3.9}$$

To solve the equations we once again decouple them by assuming that the phonon times are much faster than the quasiparticle recombination times. This would mean that the quasiparticle system is the slower system and dominates the decay. As there are phonons being created with the recombination of quasiparticles these will then immediately either escape or break another Cooper pair. This means that the number of phonons will stay very close to equilibrium and all small changes immediately vanish. Hence the number of phonons is in a quasi-equilibrium state. Thus we assume that $\frac{d\delta N_\omega}{dt} \approx 0$. This gives us the following relation:

$$\delta N_\omega = -\frac{1}{2\Gamma_{es}}\frac{d\delta N_{qp}}{dt}. \tag{3.10}$$

Filling this in in the equation for $\frac{d\delta N_{qp}}{dt}$ we get,

$$\left(1+\frac{\Gamma_B}{\Gamma_{es}}\right)\frac{d\delta N_{qp}}{dt} = -\frac{R}{V}\delta N_{qp}^2 - 2\Gamma_R\delta N_{qp}. \tag{3.11}$$

where we see that we can separate the variables,

$$\frac{1}{\frac{R}{V}\delta N_{qp}^2 + 2\Gamma_R\delta N_{qp}}d\delta N_{qp} = -\frac{1}{1+\frac{\Gamma_B}{\Gamma_{es}}}dt. \tag{3.12}$$

To integrate this, for the left part of the equation, means that we have to do a partial fraction decomposition. By doing this and integrating we get,

$$\ln\left(\frac{\delta N_{qp}}{R/V\delta N_{qp}+2\Gamma_R}\right) = -\frac{2\Gamma_R}{1+\frac{\Gamma_B}{\Gamma_{es}}}t + C_1, \tag{3.13}$$

where C_1 is an integration constant. We recognize $2\Gamma_R/(1+\frac{\Gamma_B}{\Gamma_{es}})$ as $\Gamma^*_{qp} = 1/\tau^*_{qp}$ so writing it out in terms of excess quasiparticles:

$$\frac{\delta N_{qp}}{R/V\delta N_{qp}+2\Gamma_R} = e^{t/\tau^*_{qp}+C_1} \quad \Rightarrow \quad \delta N_{qp}(t) = \frac{2\Gamma_R}{C_2 e^{t/\tau^*_{qp}} - R/V}, \tag{3.14}$$

where we made a new constant by setting $C_2 = e^{c_1}$. Filling in $t = 0$ gives us the value for the second integration constant: $C_2 = R/V + 2\Gamma_R\frac{1}{\delta N_{qp}(0)}$. Using this we get to the final equation for δN_{qp}:

$$\delta N_{qp}(t) = \frac{2\Gamma_R}{(R/V+2\Gamma_R\frac{1}{\delta N_{qp}(0)})e^{t/\tau^*_{qp}} - R/V} \quad \Rightarrow \quad \delta N_{qp}(t) = \frac{2N^0_{qp}}{(1+2N^0_{qp}/\delta N_{qp}(0))e^{t/\tau^*_{qp}} - 1}, \tag{3.15}$$

where we used the fact that $\Gamma_R = RN^0_{qp}/V$.
Looking at the found expression for the excess amount of quasiparticles, we can retrieve the two regimes of the quasiparticle decay. If $N^0_{qp}/\delta N_{qp}(0) \ll 1$ then we get the equation:

$$\delta N_{qp}(t) \approx \frac{2N^0_{qp}}{e^{t/\tau^*_{qp}} - 1}, \tag{3.16}$$

which behaves as $1/t$ for times $t \ll \tau^*_{qp}$. This is what we expect from theory and what we saw from the numerical solution for low temperatures. Then if $N^0_{qp}/\delta N_{qp}(0) \gg 1$ we get the expected equation of an exponential:

$$\delta N_{qp}(t) \approx 2N^0_{qp}e^{-t/\tau^*_{qp}}. \tag{3.17}$$

Now we will take a look at how the $1/t$ model matches the numerical solution. Firstly figure 3.3 shows that the $1/t$ model works perfectly for both temperature regimes. It can be seen how just as expected at the beginning of the curve the decay exhibits $1/t$ behavior and later on will switch to exponential behavior.

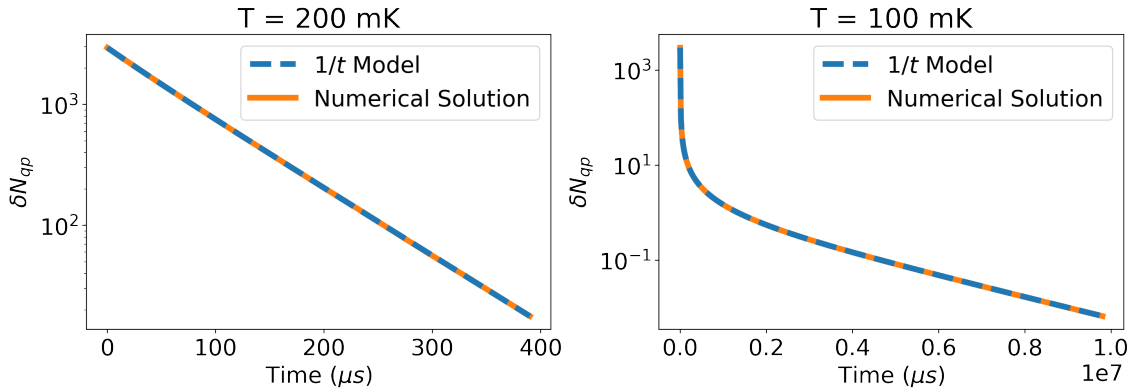

Figure 3.3: A comparison of the $1/t$ model with a numerical solution of the Rothwarf-Taylor equations for different temperatures.

Secondly looking at the phonon versus quasiparticle lifetime regimes we expect the same as for the exponential model: when the approximation, $\Gamma_R \ll \Gamma_B + \Gamma_{es}$, does not work the model breaks down. This is also what we see in figure 3.4.

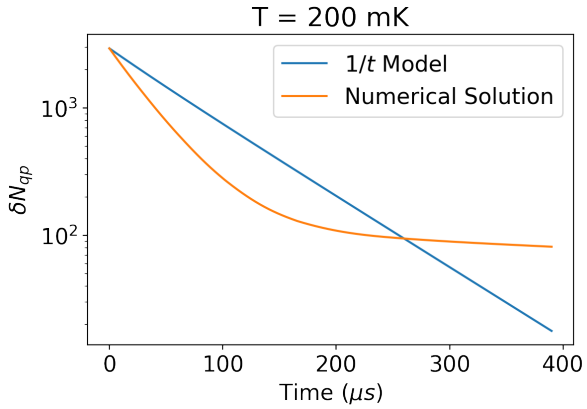

Figure 3.4: A comparison of the $1/t$ model with a numerical solution of the Rothwarf-Taylor equations for different temperatures.

3.3. Response time

The KIDs are resonators meaning that they will also have a certain response time τ_r to the photon pulse. This response time we take as the resonator ring time: $\tau_{ring} = \frac{Q}{\pi f_0}$, where Q is the loaded quality factor of the system. This response time is put into the model as a convolution with an exponential of time τ_r as,

$$(R, X)(t) = s(t) * u(t - t_d)e^{-(t-t_d)/\tau_r}, \tag{3.18}$$

where $(R, X)(t)$ is the signal used with the response time, $s(t)$ is the model signal without response time, $u(t)$ is the unit step function and t_d is the delay of the pulse.

4

Results and Discussion

We have analyzed the data of two chips called LT192chipX and LT243chipA which we will abbreviate as Chip 1 and 2 respectively. Chip 1 has been measured at different temperatures and photon wavelengths and Chip 2 has only been measured at different photon wavelengths. A chip consists of multiple KIDs as can be seen in figure 2.3. The measurements have been done at certain read-out powers which will also always be specified. Lastly, as was explained in chapter 2 all data will be analyzed in (R, X) coordinates.
The pulses shown are an average of around a thousand single photon pulses to filter out noise.

The first interesting observation that can be made about the data is the fact that read-out powers influence the pulse shape. This is shown in figure 4.1 where KID 2 on chip 2 has been measured at different read-out powers for the same temperature and wavelength. It seems that the higher the read-out power, the longer the quasiparticle decay takes.
From figure 4.1 it can be seen that the decay speed at the end of the pulse is the same for all read-out powers, the difference in shape comes from the beginning of the pulse which might mean that there is something going on with the response time of the system. For now, only low read-out powers will be looked at to ensure no effects from the read-out power will influence the data analysis.

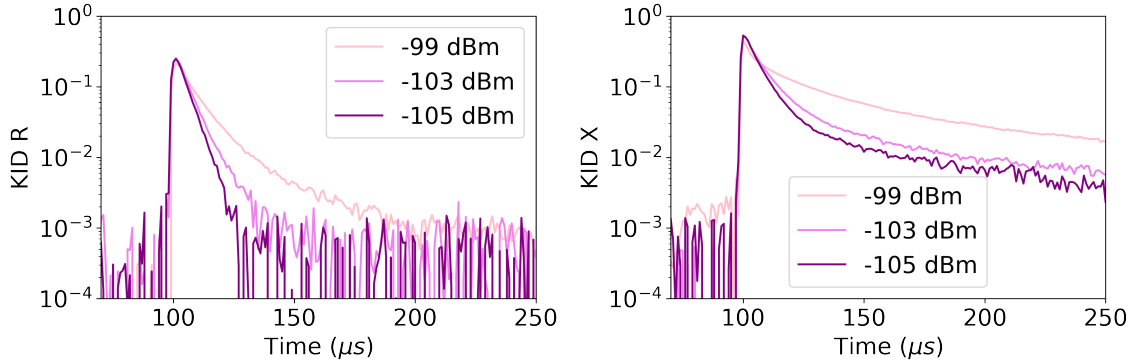

Figure 4.1: Averaged single photon pulses measured on Chip 2, KID 2 at different read out powers at a temperature of 18 mK, and a photon wavelength of 673 nm.

Some examples of the temperature- and wavelength-dependent data are shown in figures 4.2 and 4.3 respectively.

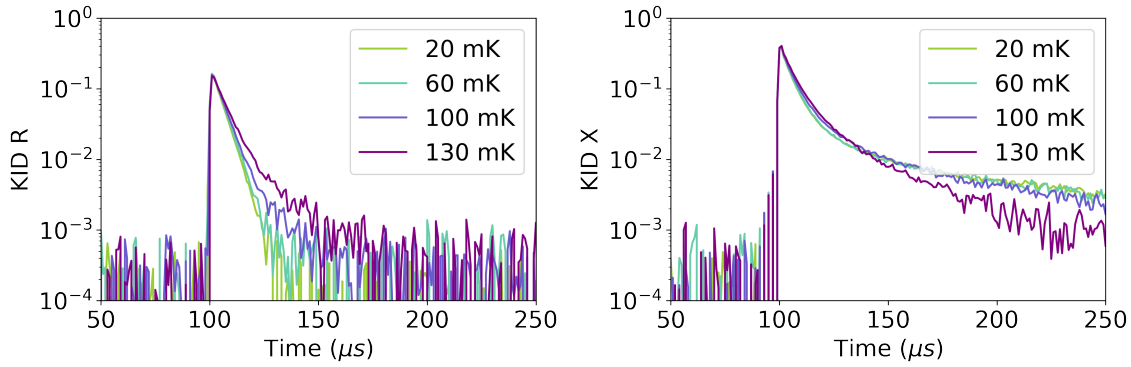

Figure 4.2: Averaged single photon pulses measured on Chip 1, KID 11 at different temperatures with a photon wavelength of 1545 nm with a read-out power of -105 dBm.

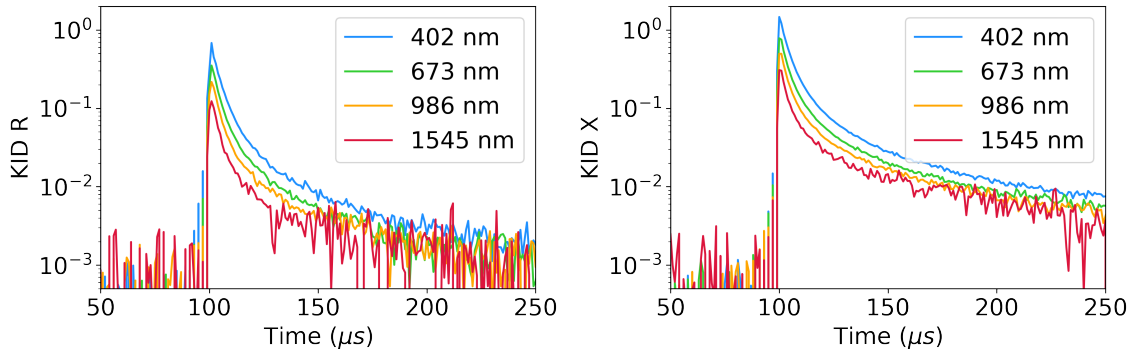

Figure 4.3: Averaged single photon pulses measured on Chip 2, KID 2 at different wavelengths photon pulses at a temperature of 18 mK and with a read-out power of -105 dBm.

We can immediately see some interesting properties of the data. For the temperature-dependent data of chip 1, the R pulse shows single exponential behavior and this is not the case for X. This behavior is found on all the KIDs of chip 1 for all wavelengths and temperatures.
For the wavelength-dependent data of Chip 2, there seems to be the same behavior for both R and X.

This difference in the R and X coordinate is contradictory to the basic model of quasiparticle dynamics and the MKID theory. As there are more quasiparticles there should be fewer Cooper pairs in the same amount by a factor of 2. This means that σ_1 and σ_2 should show the same changes. This then also means that the two coordinates should also behave the same.
Secondly, the data from chips 1 and 2 differ, and the cause for this is unknown. We will fit the double exponential and the $1/t$ model on the single photon pulses and try to deduce information from there.

4.1. Double Exponential Model

We will now take a look at the double exponential model from equation 3.4 as a fit for the single photon pulses from the data. The fit formula is given by,

$$\delta(X,R)(t) = ae^{-t/\tau_-} + be^{-t/\tau_+}, \tag{4.1}$$

where a, b, τ_-, and τ_+ are all fit parameters. τ_- is the slow lifetime and τ_+ is the fast lifetime. The two lifetimes in formula 4.1 are not known as the systems are not decoupled. This is why compared to the last model we will not be able to compare the fit parameters to the theory. We will leave all four parameters a, b, τ_-, and τ_+ as free fit parameters to see if this model can potentially fit the data.

4.1.1. Fit Procedure and fits

With the double exponential model, we expect that there are two exponentials in the curve. One at the start of the curve and one at the end. These are both individually fitted with a single exponential to extract the lifetime. An example of this is shown in figure 4.4.
We decide to only take the lifetimes from the X pulses as the R pulses don't show double exponential behavior.

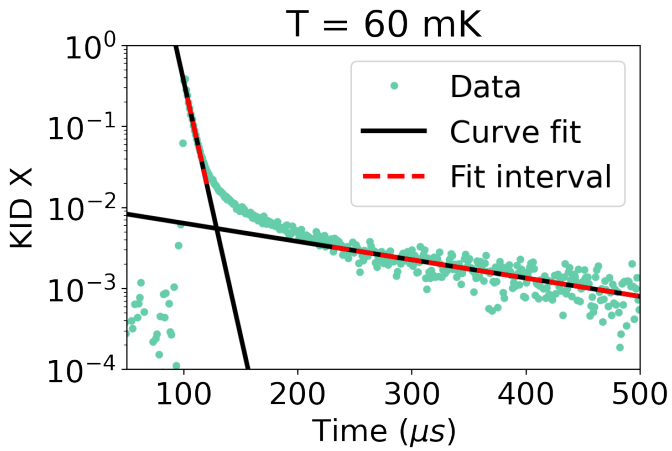

Figure 4.4: Curve fit of the double exponential model to obtain the two lifetimes in the single photon pulse. The data comes from Chip 1, KID 11 at a temperature of 60 mK at a wavelength of 1545 nm and with a read-out power of -105 dBm.

For the double exponential model, we can see the fits in for the temperature-dependent data in figure 4.5 and for the wavelength-dependent data in figure 4.6. For the temperature-dependent data of chip 1, there are no fits for the R coordinate so only two fits at different temperatures for the X coordinate are shown. The wavelength-dependent data does have fits for both coordinates which are shown for two different wavelengths.
Looking at the fits one can clearly see that the double exponential model does not fit the shape of the pulses in any case. Apart from the figures shown here, this is true for all temperatures and wavelengths also on different KIDs. Thus we come to the conclusion that the double exponential model is not a good model for the single photon pulses we're seeing.

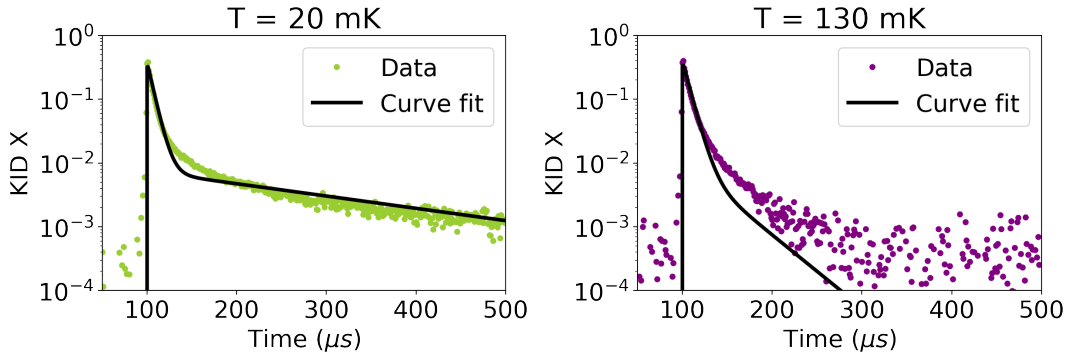

Figure 4.5: Two fits of the double exponential model to the data of chip 1, KID 11 at two different temperatures with a photon wavelength of 1545 nm and a read-out power of -105 dBm.(Only for the X coordinate)

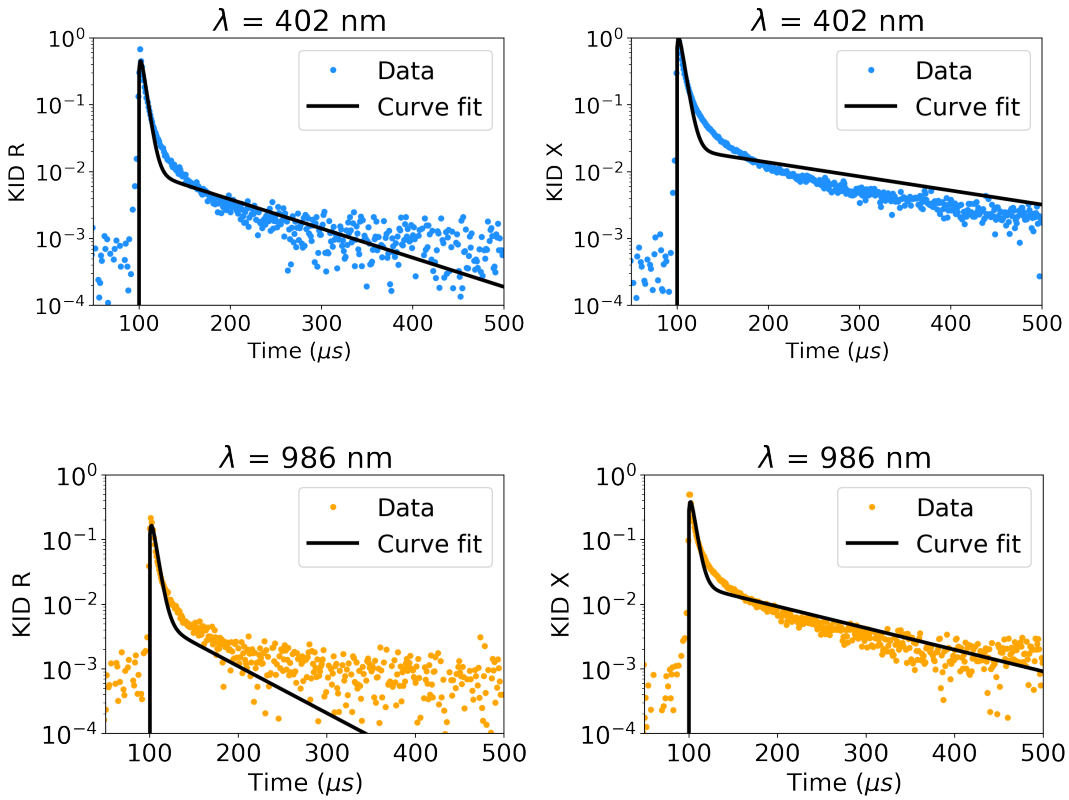

Figure 4.6: Two fits of the double exponential model to the data of chip 2, KID 15 at two different wavelengths at a temperature of 18 mK and a read-out power of -105 dBm.

4.1.2. Fit Parameters

The obtained lifetimes from the double exponential fits are plotted against temperature and wavelength in figure 4.7 where on the left is the temperature dependence and on the right is the wavelength dependence. A theory line for τ_{qp}^* is also shown in figure 4.12. The theory line has been scaled to cross the τ_+ point at 160 mK to show the difference in temperature relation.
Lastly, the region from 170 mK until 190 mK has been marked. These are the points where the X pulses start showing single exponential behavior.

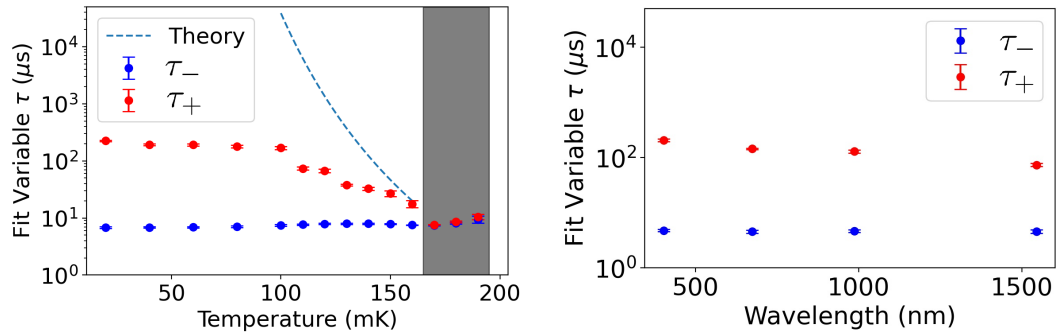

Figure 4.7: The two lifetimes of the double exponential fit are plotted against temperature in the left graph and against wavelength in the right graph. The marked region in the left plot is where the data becomes a single exponential. For the temperature dependence, a theory line for τ_{qp}^* has been provided.

As we can see in the left plot of figure 4.7 τ_- stays very constant with temperature and eventually the two lifetimes match up which makes sense as we take the same lifetime there from the single exponential. The τ_+ shows very different behavior from the theory for τ_{qp}^*. It seems to saturate below 100 mK. For the wavelength dependence on the right figure, we see that both lifetimes stay within a factor of 2.

4.2. The $1/t$ model

The $1/t$ model as was shown in formula 3.15 will now be fitted to the data. In formula 4.2 the fitting formula is given with fit parameters A and B.

$$\delta(X,R)(t) = \frac{A}{(1+B)e^{t/\tau^*_{qp}} - 1}. \tag{4.2}$$

The fit parameters have the following correspondences to the model,

$$\begin{aligned} A &= 2\frac{\partial(R,X)}{\partial N_{qp}} N^0_{qp}, \\ B &= 2\frac{N^0_{qp}}{\delta N_{qp}(0)}, \end{aligned} \tag{4.3}$$

where (R,X) is one of the coordinates of the data of the single photon pulse and $\frac{\partial(R,X)}{\partial N_{qp}}$ is given by formula 2.13.

4.2.1. Fit Procedure and Fits

As we saw in Chapter 3 the $1/t$ model in the limit of long times and low amounts of excess quasiparticles should behave like a single exponential. This means that we can find the apparent quasiparticle lifetime by fitting a single exponential to the ”tail” of the pulse. An example is shown in figure 4.8.

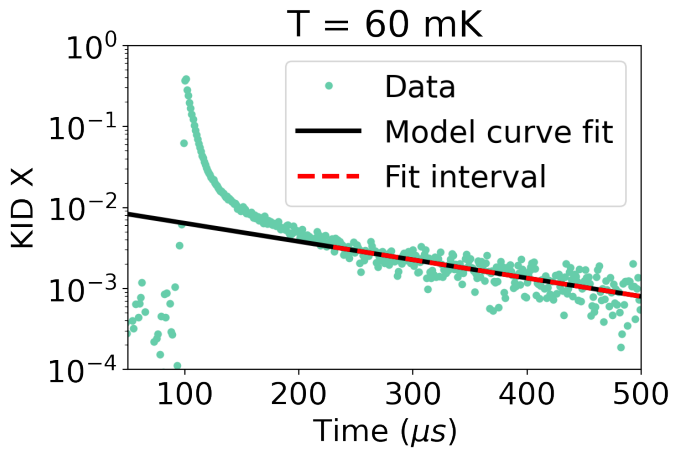

Figure 4.8: Fitting the tail of a single photon pulse to obtain τ^*_{qp}. This is done on the data from chip 1, KID 11 at 40 mK with a photon wavelength of 1545 nm and a read-out power of -105 dBm.

We choose to obtain the quasiparticle lifetime τ^*_{qp} always from the X data. This is for multiple reasons: first of all, for the R data of chip 1 there is no tail and we don't know what the lifetime of its exponential decay is so it doesn't make sense to obtain one from there. Secondly, the signal-to-noise ratio of the X data is better and lastly, it is done to be able to compare the two coordinates. As the theory of our model says that the lifetimes of the two coordinates should be the same. We can compare this by using the same lifetime for both of the coordinates.

First, we made the attempt to calculate the number of quasiparticles by theory from the quasiparticle lifetime using equation 2.5. Then also the number of excess quasiparticles from the pulse was calculated from the energy of the photon and the energy of the Cooper pairs. From there only the scaling factor A from equation 4.3 needed to be fitted as a conversion from the number of quasiparticles to the specific coordinate. This resulted in figure 4.9 which shows that for both R and X this is clearly not the way to go. This we could have expected as the theory of the lifetime did not match the found lifetimes as we saw in figure 4.12.

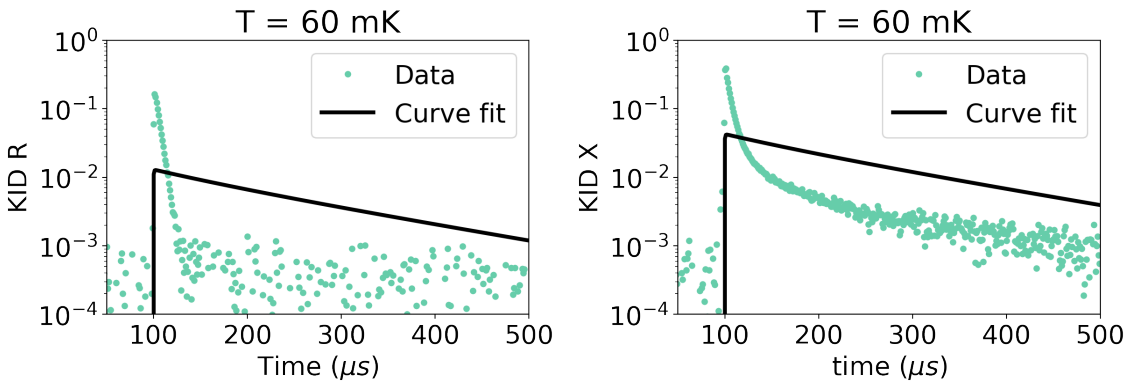

Figure 4.9: $1/t$ curve fit where N_{qp}^0 was calculated from the lifetime from the curve fit. Data from chip 1, KID 11 at 40 mK with a photon wavelength of 1545 nm and a read-out power of -105 dBm.

So then it was decided to leave both the parameters N_{qp}^0 and δN_{qp} as free parameters to see if this function could make for a good fit. This would mean using equation 4.2 as a fit function with both A and B as free parameters. First, we will take a look at the temperature-dependent data. The results of this are shown in figure 4.10.
For the R coordinate, it is very clear the fit does not work and shows the difference in lifetime compared to the X coordinate data. For the X data it gets pretty close but the shape still differs. It seems like the first decay takes longer in the data than in the model. At higher temperature, the X data shows single exponential behavior it was chosen to take the first exponential as lifetime.

Secondly, we look at the wavelength-dependent data in figure 4.11. For the wavelength-dependent data, the R and X coordinates are more alike thus the $1/t$ fit works better here for the R coordinate. It shows a very good fit for the X coordinate, especially for lower wavelengths. However, interestingly here the data compared to the fits seems to shift with wavelength. For lower wavelength and thus higher energies, the $1/t$ model works very well and the first fast decay seems to take longer in the data. At higher wavelengths or lower energies, the fit seems to start to become worse as it undershoots with a first decay that takes too long. This would mean that the length of the first decay is pulse height dependent. It would mean that there is something going on with the first decay that our model is not taking into account.

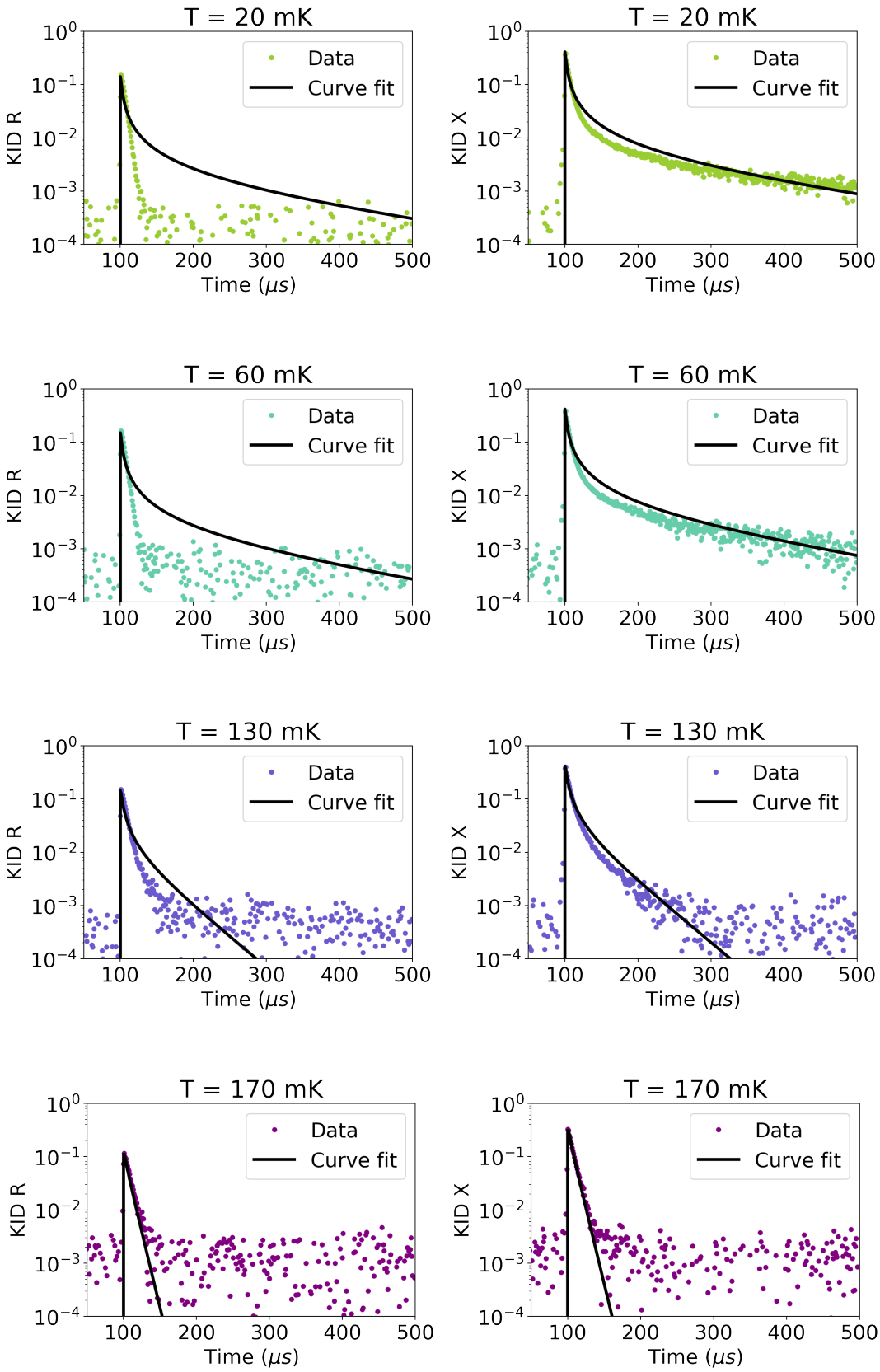

Figure 4.10: Curve fit of the $1/t$ model for the temperature-dependent data of Chip 1, KID 11 at a wavelength of 1545 nm, and a read-out power of -105 dBm.

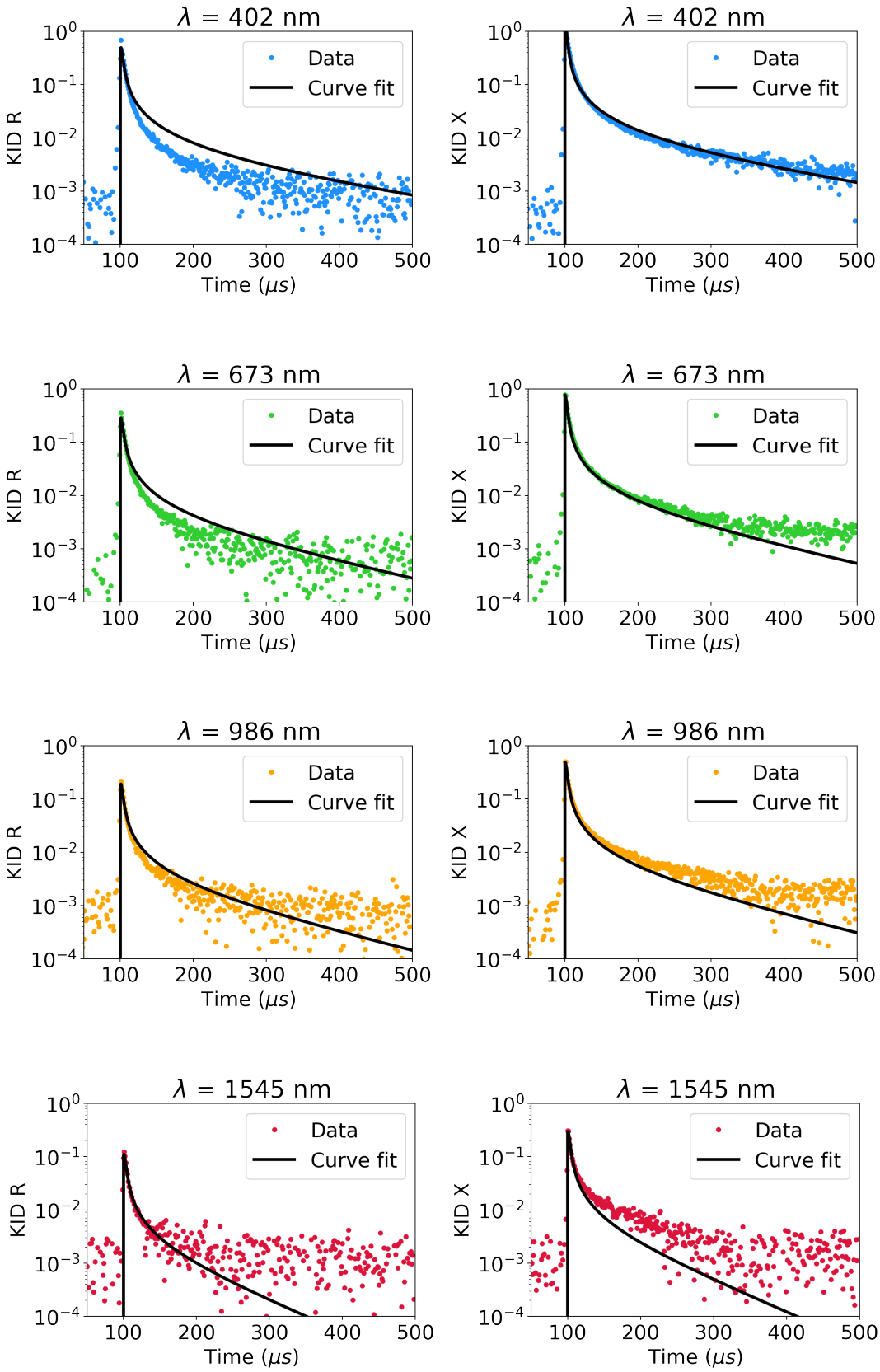

Figure 4.11: Curve fit of the $1/t$ model for the wavelength-dependent data of Chip 2, KID 15 at a temperature of 18 mK, and a read-out power of -105 dBm.

4.2.2. Fit Parameters

The obtained lifetimes can be found in figure 4.12 for the temperature and wavelength-dependent data. A theory line is drawn from equation 2.5 in the left figure from 4.12. It is scaled to match the last point of the fitted τ^*_{qp} to be able to clearly show the clear difference in temperature dependence.

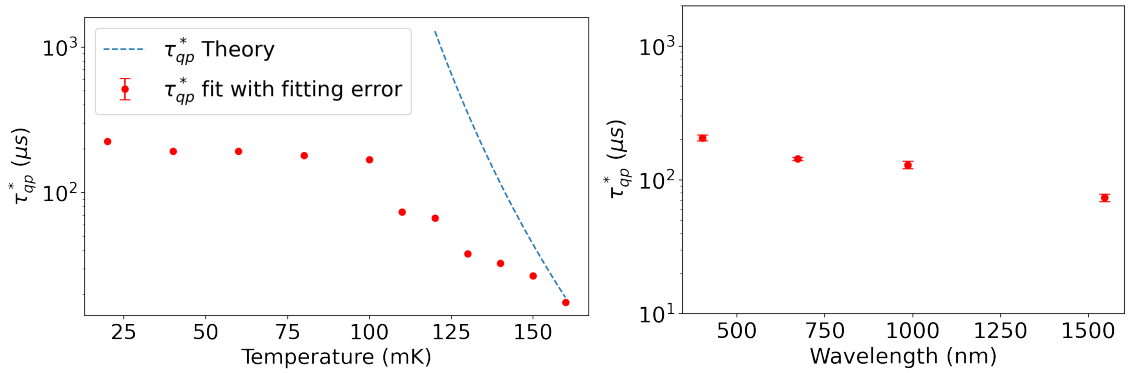

Figure 4.12: The obtained lifetimes τ^*_{qp} plotted versus temperature and wavelength. The temperature-dependent graph on the left also has a theory line which is scaled to match the last point. The data is from all temperatures of chip 1, KID 11 at -105 dBm, and all photon wavelengths of chip 2, KID 15 at -105 dBm.

Considering the temperature dependence of τ^*_{qp} we expect the lifetime to go up as the temperature goes down. This does happen in the left plot in figure 4.12 however if we compare it to the theory line it should happen a lot faster. It seems as if the lifetime saturates for low temperatures which is also seen in [18], [19]. There the suggestions are made that either the saturation of the quasiparticle lifetime is due to the presence of a relaxation channel, which is not caused by the conventional process dominated by electron-phonon interaction [18] or that the quasiparticle lifetime saturation is due to a saturation in the quasiparticle density [19].
For the wavelength dependence, we expect the lifetime to stay constant as the temperature also stays constant. In the right plot of figure 4.12 we can see that the lifetime doesn't stay within a factor 2 and seems to exhibit a wavelength dependence.

The fit parameters A and B that were obtained from the fits in the last section are plotted against temperature and against wavelength in figure 4.13.

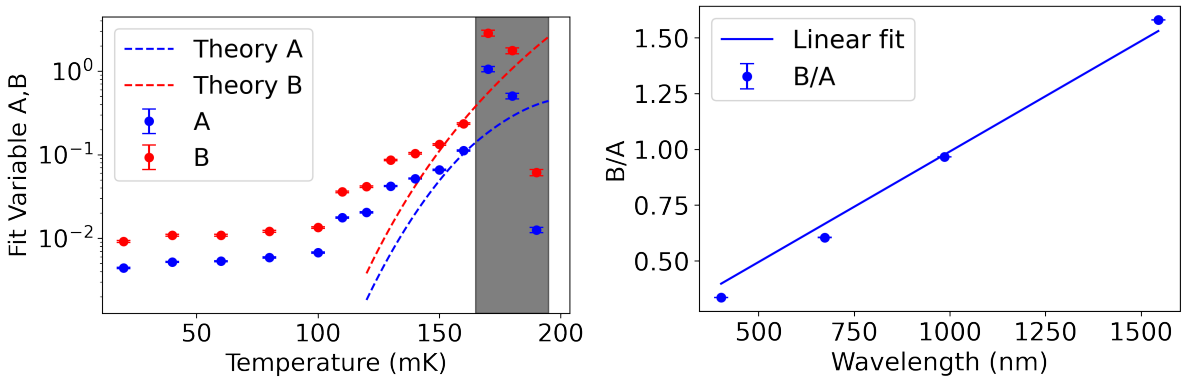

Figure 4.13: The fit parameters of the $1/t$ fit A and B plotted against temperature in the left graph and against wavelength in the right graph. The marked region in the left plot is where the data becomes a single exponential. For the temperature dependence theory lines for A and B are shown.

A and B are both dependent on N^0_{qp} as in equation 4.3. That means they would have the same temperature dependence. However, A is also dependent on the responsivity between the number of quasiparticles and the measurement coordinate. This scaling factor is dependent on the Q-factor which does change with temperature. At high temperatures, the Q-factor will go down because of the increased

amount of quasiparticles. So the scaling factor would also go down for higher temperatures and so will A. This can be seen in the left plot in figure 4.13. In the fit parameters and the theory line.
The fit variables A and B don't fit the theory as for low temperatures they both seem to saturate. This is probably because of the same thermal quasiparticle saturation as was talked about for the τ^*_{qp}. For high temperatures, we observe a single exponential thus the results for A and B are clearly not reasonable. The wavelength dependence of $B/A = 1/\delta N_{qp}(0)\frac{\delta(R,X)}{\delta N_{qp}}$ is shown in the right plot of figure 4.13. This should have a linear wavelength dependence as with higher wavelength the amount of quasiparticles increases and thus B increases again. That is exactly what we see as B/A increases linearly with the wavelength. A linear curve fit, $y = ax$, is also plotted with the B/A points to show the linear dependence. The linear offset should be zero because when the wavelength decreases the number of quasiparticles should increase to the point where $B \propto 1/\delta N_{qp}(0) \to 0$.

4.3. The $1/t$ Model With a Different Response Time

We have seen how the first part of the single photon pulse doesn't match our $1/t$ model. There seems to be a different time constant at the beginning of the curve. This might be the response time as this changes the behavior of the first part of the single photon pulse.
Thus we decide to try and fit a new response time. First, we fit the quasiparticle lifetime the same way as before by fitting it to the tail of the pulse. But then the problem is that the variables A and B are very dependent on the response time. This means that changing one is going to change the other a lot. So trying to fit all three parameters at once does not work. This is why we fit them iteratively. We start with the response time from theory which we took as the resonator ring time: $\tau_r = \tau_{ring} = \frac{Q}{\pi f_0}$ and then we fit A and B. With these parameters, we fit a new response time and from there we fit new A and B and keep repeating until the difference between the new iteration and the last one is smaller than 10^{-4}.

With this method, we obtained new response times for the systems. Firstly we look at the results for the temperature-dependent data. This first had a ring time of $\tau_{ring} = 0.52$ μs. Four fits at different temperatures with a new response time can be seen in figure 4.15.

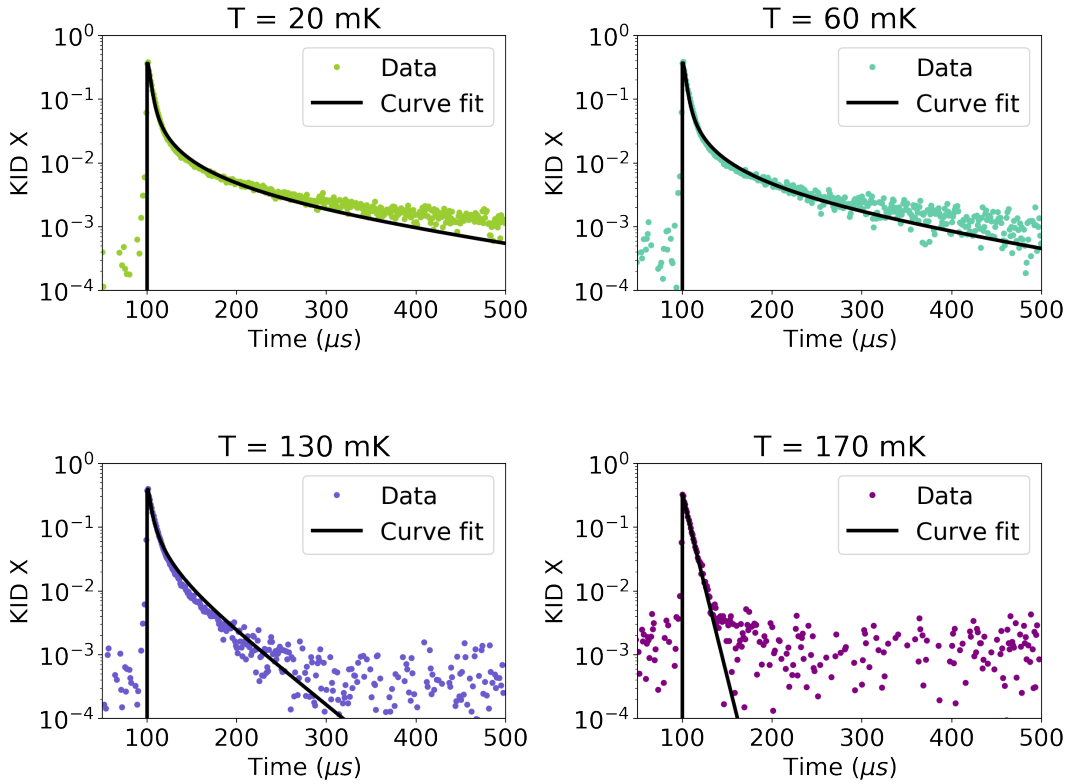

Figure 4.15: Fits of the $1/t$ model with a different response time that was fit iteratively. The data is from chip 1, KID 11 at -105 dBm.

The beginning of the curve fits a lot better with a new response time. Especially for the lower temperatures does it seem to do very well. We do see that at the end of the curve there is a small undershoot.

Next, we can take a look at the wavelength-dependent data for the X and R coordinate with new response times in figure 4.16. Here the found fit response time was different for every photon wavelength. The original calculated response time of the system was 1.5 μs. The found lifetimes from the fits of every pulse can be seen in figure 4.17.

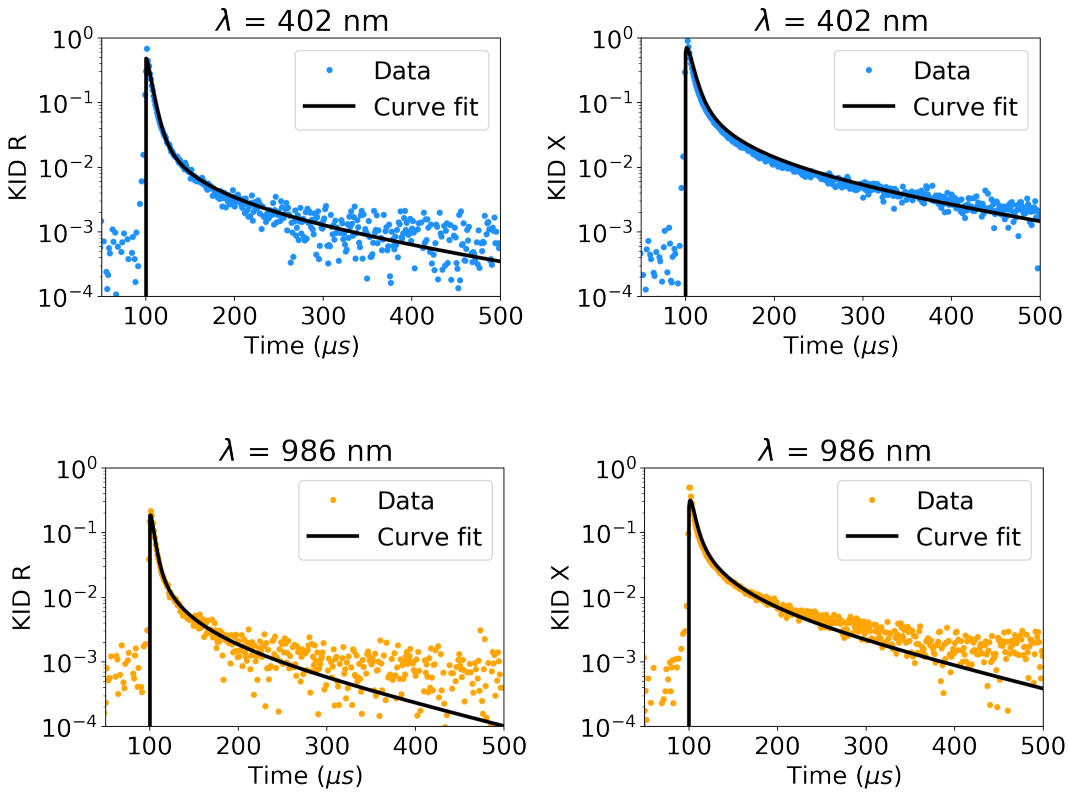

Figure 4.16: Fits of the $1/t$ model with a different response time that was fit iteratively. The data is from chip 2, KID 15 at -105 dBm.

Also for the wavelength-dependent data, a different response time seems to improve the curve fits a lot. The found lifetimes from both the temperature-dependent and wavelength-dependent data from every pulse can be seen in figure 4.17.

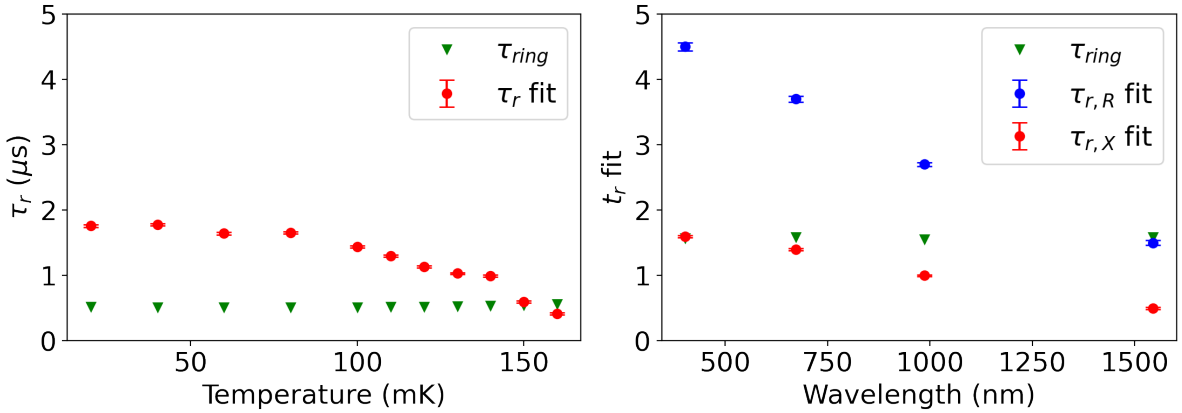

Figure 4.17: $1/t$ model with fit response time. The data is from all temperatures of chip 1, KID 11 at -105 dBm, and all photon wavelengths of chip 2, KID 15 at -105 dBm.

The temperatures from 170 to 190 mK are not shown in the left graph of figure 4.17 as these pulses are single exponential thus no response time can be determined. From the right graph in figure 4.17 we can see a wavelength dependence for the response time which seems to be linear. Looking at the response time versus the temperature it seems that for low temperatures it stays constant and at higher temperatures, it becomes faster.
The new A and B fit parameters still show the same temperature and wavelength relations.
The hypothesis for these different lifetimes is that there is another response time in the system that slows everything down apart from the ring time of the resonator $t_{ring} = \frac{Q}{\pi f_0}$. We think this comes from a relaxation time immediately after the photon hits the superconductor. We are looking at a disordered superconductor this means that the structure inside the superconductor can lead to very unequally distributed quasiparticles. These quasiparticles would then first have to distribute throughout the superconductor before they could recombine into Cooper pairs effectively. This would explain the wavelength dependence as creating more quasiparticles at higher energies would take create a longer relaxation time.

5

Conclusion and Recommendations

At the start of this thesis, we aimed to find a model that could explain the shape of the single photon pulses of β-Ta. To start we made several models to explain the behavior of the quasiparticle dynamics in the superconductor. After that, we compared these models to single photon pulses from the data of two chips. We first looked at the double exponential model and saw that it did not fit well with the single photon pulses. Therefore, we conclude that the single photon pulse shape is not due to the assumption of $\Gamma_R \ll \Gamma_B + \Gamma_{es}$ being broken.

From there we moved on to the $1/t$ model. It became clear that we could not use calculated parameters N_{qp}^0 and τ_{qp}^* from theory as they were vastly different from the ones in the single photon pulses of the data. For this reason, we decided to leave all the variables in the fit free except the quasiparticle lifetime which was obtained from the tail of the single photon pulse. This seemed to fit better than the double exponential model but in the first decay, there was a difference with the pulses from the data.

Most of the extracted parameters from the fits didn't follow the theory. Firstly the obtained lifetimes were a lot smaller than our theory suggests. In other works [18], [19] it is also seen that the lifetimes saturate and don't correspond to the theory in low temperatures, but here it is also for high temperatures.
Secondly, the fit parameters of the $1/t$ model didn't show the temperature dependence we would expect. They both also saturate at low temperatures. From this, we conclude that the saturation of the lifetime must come from a saturation in quasiparticles.
For the wavelength dependence of the variables, we did get the expected linear wavelength relation of B/A.

Since the $1/t$ model looked promising but didn't completely fit yet we proposed a different response time. When we fit the response time as well we obtained very good fits for the single photon pulses. The extracted lifetimes seemed to be linearly wavelength dependent. From this, we can conclude that for a higher energy pulse there is a longer response time. For the temperature dependence, the response time remains constant and then drops for higher temperatures. We think this is because as the temperature rises there are more quasiparticles for the system to respond faster to the pulse. Lastly, we saw a big difference in response time between the coordinates R and X in the wavelength-dependent data. This could have to something with the fact that they measure two different things: quasiparticles and Cooper pairs. Or because the responsivity of the two coordinates is also different.

We finally conclude that the $1/t$ model with adjusted response time is the best model to explain the single photon pulses of β-Ta. This means that the quasiparticle system first shows $1/t$ behavior in the low-temperature regime and at the end of the pulse exponential behavior.

For following research we recommend looking at the following:

1. The difference in response times from theory.
2. The position dependence of parameters in the superconductor.
3. Pulse shape effects at different read-out powers.
4. Different behavior in different materials.

Firstly, we don't know where the difference in response times from theory comes from. It is therefore recommended to look further into this.
Secondly, β-Ta is a disordered superconductor which means there is a position dependence of parameters in the superconductor. From these position dependencies uneven distributions of quasiparticles could emerge directly after the photon pulse which would create a longer relaxation and thus response time. It will be interesting to see if these position dependencies can significantly change the photon pulse shapes.
Thirdly, at different read-out powers, the single photon pulses showed different shapes which could have something to do with the response times.
And lastly, looking at different materials will give more information if for example these properties are also observed in aluminium.

Bibliography

[1] K. Kouwenhoven, D. Fan, E. Biancalani, *et al.*, *Resolving Power of Visible to Near-Infrared Hybrid beta-Ta/NbTiN Kinetic Inductance Detectors*, arXiv:2207.05534 [astro-ph, physics:cond-mat, physics:physics], 2022.

[2] M. Lesser, "A summary of charge-coupled devices for astronomy," *Publications of the Astronomical Society of the Pacific*, vol. 127, no. 957, p. 1097, 2015. DOI: 10.1086/684054.

[3] A. Endo, K. Karatsu, Y. Tamura, *et al.*, "First light demonstration of the integrated superconducting spectrometer," en, *Nat Astron*, vol. 3, no. 11, pp. 989–996, 2019, Number: 11 Publisher: Nature Publishing Group, ISSN: 2397-3366.

[4] D. van Delft and P. Kes, "The discovery of superconductivity," *Physics Today*, vol. 63, no. 9, pp. 38–43, 2010, Publisher: American Institute of Physics, ISSN: 0031-9228.

[5] J. Bardeen, L. N. Cooper, and J. R. Schrieffer, "Microscopic theory of superconductivity," *Phys. Rev.*, vol. 106, pp. 162–164, 1 1957.

[6] J. Bardeen, L. N. Cooper, and J. R. Schrieffer, "Theory of superconductivity," *Phys. Rev.*, vol. 108, pp. 1175–1204, 5 1957.

[7] L. Damaris, *New roads opening in the field of superconducting materials after the discovery of mgb 2*, 2012.

[8] P. J. D. Visser, "Quasiparticle dynamics in aluminium superconducting microwave resonators," en, *Delft University of Technology*, 2014.

[9] A. Rothwarf and B. N. Taylor, "Measurement of recombination lifetimes in superconductors," *Phys. Rev. Lett.*, vol. 19, pp. 27–30, 1 1967.

[10] S. B. Kaplan, C. C. Chi, D. N. Langenberg, J. J. Chang, S. Jafarey, and D. J. Scalapino, "Quasiparticle and phonon lifetimes in superconductors," *Phys. Rev. B*, vol. 14, pp. 4854–4873, 11 1976.

[11] P. J. de Visser, J. J. A. Baselmans, S. J. C. Yates, P. Diener, A. Endo, and T. M. Klapwijk, "Microwave-induced excess quasiparticles in superconducting resonators measured through correlated conductivity fluctuations," *Applied Physics Letters*, vol. 100, no. 16, p. 162 601, 2012, Publisher: American Institute of Physics, ISSN: 0003-6951.

[12] P. J. de Visser, S. A. de Rooij, V. Murugesan, D. J. Thoen, and J. J. Baselmans, "Phonon-Trapping-Enhanced Energy Resolution in Superconducting Single-Photon Detectors," *Physical Review Applied*, vol. 16, no. 3, p. 034 051, 2021, Publisher: American Physical Society.

[13] D. C. Mattis and J. Bardeen, "Theory of the anomalous skin effect in normal and superconducting metals," *Phys. Rev.*, vol. 111, pp. 412–417, 2 1958.

[14] R. Barends, "Photon-detecting superconducting resonators," en, 2009, Publisher: R. Barends.

[15] S. de Rooij, "Quasiparticle Dynamics in Optical MKIDs: Single Photon Response and Temperture Dependent Generation-Recombination Noise," en, 2020.

[16] C.-C. Su, "Microwave Engineering, 4th Edition," en,

[17] N. Zobrist, N. Klimovich, B. Eom, *et al.*, "Improving the dynamic range of single photon counting kinetic inductance detectors," *JATIS*, vol. 7, no. 1, p. 010 501, 2021, Publisher: SPIE, ISSN: 2329-4124, 2329-4221.

[18] R. Barends, J. J. A. Baselmans, S. J. C. Yates, J. R. Gao, J. N. Hovenier, and T. M. Klapwijk, "Quasiparticle relaxation in optically excited high-Q superconducting resonators," *Physical Review Letters*, vol. 100, no. 25, p. 257 002, 2008, arXiv:0802.0640 [cond-mat], ISSN: 0031-9007, 1079-7114.

[19] P. J. de Visser, J. J. A. Baselmans, P. Diener, S. J. C. Yates, A. Endo, and T. M. Klapwijk, “Number Fluctuations of Sparse Quasiparticles in a Superconductor,” *Physical Review Letters*, vol. 106, no. 16, p. 167 004, 2011, Publisher: American Physical Society.

A

Constants of the Models

Variable	Value	Unit	Description
h	4.136 $\times 10^{-3}$	μeV·μs	Planck's constant
c	2.9979 $\times 10^{8}$	μm/μs	Speed of light
K_b	86.17	μeV K^{-1}	Boltzmann's constant
T_c	1.11	K	Critical temperature
τ_0	81 $\times 10^{-3}$	μs	Phonon electron interaction time
T_D	266	K	Debye temperature
N_0	3.07 $\times 10^{4}$	μeV$^{-1} \cdot \mu$m^{-3}	Single spin electron density of states at the Fermi level
V	25	μm^3	Volume of the superconductor
Δ	168.34	μeV	Cooper pair bonding energy
τ_{pb}	0.015 $\times 10^{-3}$	μs	Pair breaking time
τ_{es}	0.02 $\times 10^{-3}$	μs	Phonon escape time

Table A.1: All the constants used in the models of chapter 3.